CCD Radiation Effects and Test Issues for Satellite Designers

Review Draft 1.0

Prepared by Cheryl J. Marshall (NASA-GSFC) and Paul W. Marshall

(NASA-GSFC Multi-Engineering Disciplinary Support Contract Task 1058)

6 October, 2003

CCD Radiation Effects and Test Issues for Satellite Designers

CCD Radiation Effects and Test Issues for Satellite Designers

I. Introduction

Charge coupled devices (CCDs) are currently the preeminent detector in the near near ultraviolet (UV) to visible wavelength region for astronomical observations in space and are essential in earth-observing space missions as well. [Blad00] Specialized scientific CCDs have also been developed for use in the UV and x-ray regimes.   CCDs have replaced the vidicon tube technology that flew on the Surveyor, Ranger, Mariner, Viking and Voyager missions. A fascinating historical account of CCDs in space may be found in Chapter 1 of [Jane01].   Much science has been performed using CCDs despite their well-known vulnerability to radiation damage. Although other visible technologies such as active pixel sensor (APS) arrays offer some advantages with respect to radiation hardness, scientific quality APS devices do not exist at present and are not expected to be available in the near future. Hence, this paper focuses on the lessons learned by the radiation effects community as to how to best characterize CCDs for use in the natural space environment.

This document is based on our experiences with numerous flight projects including SOHO, FUSE, several generations of HST instruments, CHANDRA, etc. We introduce various methods of measuring the radiation response of CCDs and discuss the application-specific nature of the charge transfer efficiency. Finally we discuss proton testing issues for flight programs. The reader is referred to several review papers [Hopk96, Pick03] as well as Janesick's excellent book entitled Scientific Charge-Coupled Devices [Jane01] for an in depth review of charge coupled device operation and its response to the radiation environment. In a follow-on document, we will address the problem of performing predictions of the on-orbit performance of CCDs.

I A. Description of CCD Technology

CCDs contain a matrix of up to several million photosensitive elements (or pixels) which generally operate by converting the photo-generated charge to a voltage that is multiplexed to a small number of output amplifiers. Present charge coupled devices (CCDs) are available with picoampere dark currents[1] and charge transfer efficiencies (CTE) in excess of 0.9999995 per pixel. Figure 1 shows the basic structure, typically an array of Si MOS capacitors built on a p-type epitaxial layer about 10-20 μm thick. Potential wells are created by applying a voltage to one of the gate electrodes. The n-

---

[1] Dark currents as low as 3 pA/cm2 have been measured at room temperature! [Jane01, p. 605]

type buried channel ensures that the potential minimum is situated ~1 μm into the silicon so that charge is kept away from the silicon-silicon dioxide interface. In the most simple CCD readouts, charge is moved from one pixel to another by switching the applied voltage from one electrode phase to the next, first vertically, one row at a time, (in parallel) to the serial register where each row is moved one pixel at a time, to a readout amplifier [Jane01]. Three or four clock phases/pixel are commonly used for vertical transfers, and two (plus an implant to define the charge transfer direction) or three for serial transfers. The charge detection amplifier provides a voltage that can be further processed.

It is critical to transfer the charge packets with minimal loss of signal electrons since a single packet may undergo several thousand transfers before reaching the output amplifier of today's very large arrays. The charge transfer efficiency (CTE) is defined to be the percentage of charge in a signal packet that is transferred from one pixel to the next, and is a key performance parameter for CCDs.

Scientific CCDs come in several different architectures which do have implications for the radiation hardness of the device. In the case of a linear shift imager, a scene is acquired by scanning it vertically past the linear array. In contrast a "full frame" area array integrates the scene, and then, once the shutter is closed, the CCD array is read out. So-called 'frame transfer' CCDs have an upper 2-dimensional array of pixels used to integrate a scene which is then quickly transferred to a second storage array that is masked with metal and has independent clocking for reading out the scene. This mode has advantages when the time required to read is on the order of the integration time since it preserves the captured image as a pure "staring mode snapshot." Note that CCDs can also be designed to have multiple readout modes utilizing more than one amplifier which can impact the radiation performance of the device.

Although CCD technology development has almost exclusively focused on the n-channel CCD (n-CCD), p-CCD devices are also being pursued for their potential to be somewhat more radiation robust [Sprat97, Hopk99, Bebe02]. For example, the Supernovae Acceleration Program (SNAP) has fabricated some potentially flight worthy high resistivity p-CCDs that show promise. The Defense Threat Reduction Agency has also fabricated some nominal resistivity p-CCDs that may be flown aboard a NASA test-bed.[2]

---

[2] For example, see http://lws-set.gsfc.nasa.gov
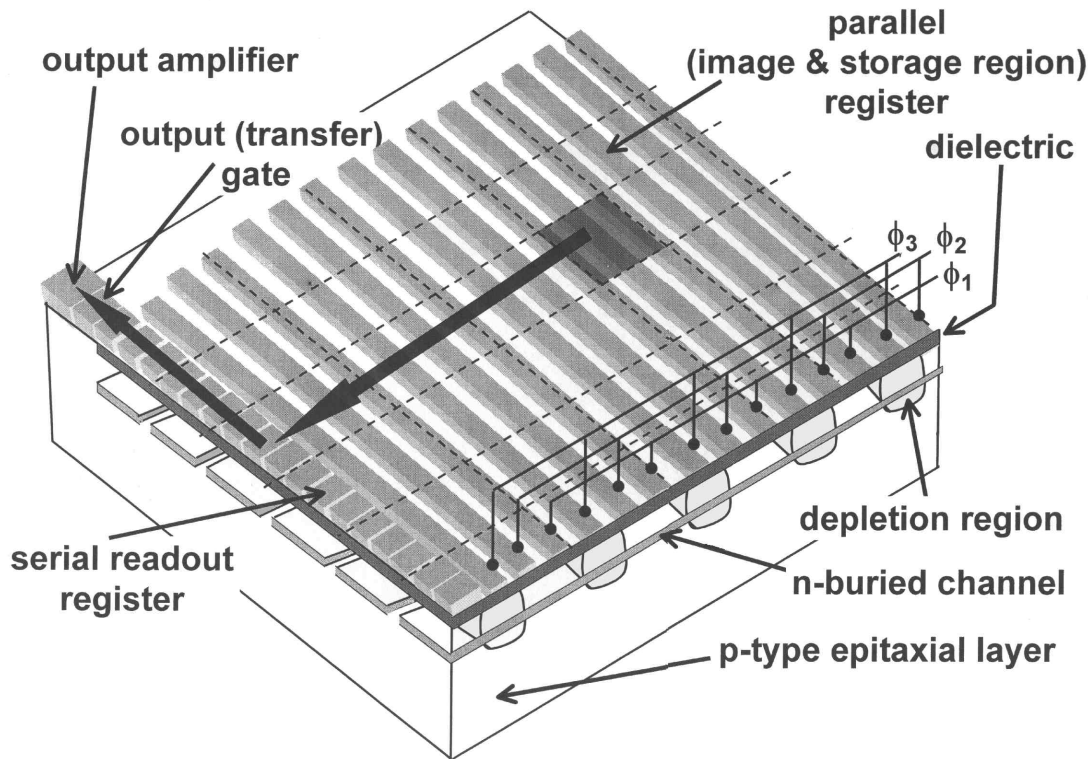
Figure 1   Illustration of parallel charge transfer down a row of MOS capacitors. A 3 phase CCD is pictured, in which each pixel is composed of 3 electrodes for charge transfer. The signal charge travels in the buried channel and is restricted to a single row by implanted channel stops.   From [Pick03].

II. Radiation Effects in CCDs

The performance of CCDs is permanently degraded by total ionizing dose (TID) and displacement damage effects. TID produces threshold voltage shifts on the CCD gates and displacement damage reduces the CTE, increases the dark current, produces dark current nonuniformities and creates random telegraph noise in individual pixels. In addition to these long term effects, cosmic ray and trapped proton transients also interfere with device operation on orbit.

II A. Total Ionizing Dose (TID)[3]

Since CCDs use the metal - insulator - semiconductor structure for either photo-detection and readout, these devices are susceptible to ionization damage within the insulator layer. Silicon dioxide is almost exclusively used as the insulator in CCDs to form a MOS structure. The main effects are the build up of trapped charge in the oxide and the generation of traps at the silicon dioxide/silicon interface. In an imager these produce shifts in flatband voltages (i.e. the effective bias voltages applied to the device are changed), increases in the surface dark current (i.e. the component of thermal dark current which is generated at the silicon dioxide/silicon interface), increased amplifier noise, and changes in linearity. These effects are relatively well understood in CCDs and can in principle be reduced by appropriate choice of device architecture and oxide technology. For example, the surface dark current contribution is effectively minimized by inverting the surface using boron multi-phase pinned (MPP) implants as described below. CCD performance in space is not generally limited by total ionizing dose effects because displacement effects are more often the limiting mechanism.

Most oxides in commercial CCDs are thick (~100 nm) and radiation-soft so that for a device biased during irradiation a typical shift in flatband voltage is ~0.08 V/krad(Si) (or roughly a third to a half that for a unbiased device) [Hopk92, Robb93]. Total voltage shifts below about 2 V can be accommodated by optimal choice of the biases before flight or irradiation. For total doses above about 5-10 krad we start to see changes in performance of the output amplifier and shifts in the clock voltage at which inversion (MPP operation) occurs towards more negative values. These effects may be registered as an increase in the observed CCD read noise. However the device will probably be functional up to several tens of krad(Si) (and perhaps to higher ionizing doses if bias voltages are adjusted in-flight). Devices have been developed with more radiation hard oxides so that performance is possible up to 1 Mrad(Si), but such devices are not generally available commercially. A degree of hardening can be achieved by thinning the dielectric layer and also by balancing the electron and hole trapping in dual oxide/nitride dielectrics. However there is often a reduction in manufacturing yield for such specialized devices.

Susceptibility to ionization damage can vary significantly depending on the CCD manufacturer and CCD technology implemented. In some cases, the ionization-induced surface dark current density can be extremely important; sometimes leading to a 'white-out' of the image if the device is operated at room temperature after receiving a few tens of krad(Si) (typical increases are in the range 1-10 mA/cm^2 at 20°C). However, if the CCD is biased so that the silicon surface is inverted, then holes from the channel stop regions fill the Si/SiO_2 interface traps and suppress the generation of dark current [Saks80]. This can be achieved with an extra implantation to form a multiphase pinned

---

[3] This section is largely adapted from G. R. Hopkinson, C. J. Dale, and P. W. Marshall, "Proton effects in CCDs", IEEE Trans. on Nucl. Sci., vol. 43, no. 2, pp. 614-627, Apr. 1996.

device [Jane95], or by shuffling the charge back and forth between gates within a pixel faster than the surface states can respond (so-called dither clocking) [Burk91], [Vant94]. Since the dark current of buried channel CCDs is dominated by carrier generation at the Si/SiO$_2$ interface, MPP operation can reduce the observed pre-irradiation dark current by more than an order of magnitude. With modern devices and optimized clocking, the loss in full well capacity with MPP devices need not be more than 20%. Use of dither clocking to swap between integration phases can result in dark current nonuniformity, but an optimized choice of clock levels can help ameliorate this problem. Note that if surface dark charge is not suppressed, then it is often found that it is increased (by a factor ~ 2) under metallizations, such as used for the storage region light shield and for masking dark reference pixels.

In summary we see that, especially for mission with requirements less than about 10 krads(Si), the TID-induced radiation response can generally be managed. However, it is important to verify that flatband shifts will not take a device out of inversion prior to the expected mission dose, and also to ensure that the readout amplifier circuitry is robust. In closing, we note that post-irradiation (i.e. annealing) effects are not usually significant for flatband shifts in CCD oxides [Hopk92], [Hopk96].

II B. Displacement Damage

Displacement damage is produced by energetic particles such as protons and neutrons which collide with silicon atoms and displace them from their lattice sites. As a result many vacancy interstitial pairs are formed, most of which recombine. The vacancies that survive migrate in the lattice and form stable defects such as the phosphorus-vacancy complex (or E-center), oxygen-vacancy defect (or A-center), divacancy, etc. These defects degrade CCD performance by decreasing the CTE, increasing the average dark current and dark current nonuniformity, by introducing individual pixels with very high dark currents (or "spikes"), and by introducing random telegraph noise in pixels. In fact, bulk displacement damage effects often dominate the radiation response in state-of-the-art scientific imagers when operated in natural particle environments. The flatband shifts and dark current increases that occur for ionizing dose levels below 10-20 krads(Si) are often not serious, and can be overcome with minor changes in voltages and operating temperature. In contrast, significant displacement damage induced CTE losses are observed for proton exposures of less than 1 krad(Si). Nevertheless, the degree of CTE loss that is tolerable is very application-dependent, and it is still possible for a device to ultimately fail as a result of either TID or displacement damage effects at higher exposure levels. A detailed description of proton effects in CCDs may be found in a recent review article [Hopk96] and references therein.

II. B. *i.* Charge Transfer Efficiency (CTE)

One of the most important performance parameters for a CCD is the CTE, which is the fraction of signal charge transferred from pixel to pixel during read out. Arrays with 1024 x 1024 pixels (and larger) are routinely used today, and require very low trap

densities in order to operate correctly. For example, to reduce signal loss to less than 10% for 1000 pixel-to-pixel transfers, a CTE of at least 0.9999/pixel is necessary. For a signal size of 1,000 electrons (typically contained within 50 μm^3), this corresponds to less than one radiation induced defect every ten pixels, which can easily be exceeded during a typical space mission [Hopk96]. If a signal charge is trapped by a proton induced defect, and remains trapped for more than one clock cycle, it will be lost from the signal charge packet. The trapped charge is eventually re-emitted into trailing pixels, and produces a smeared image. It is the interplay between the temperature dependent carrier emission and capture dynamics of the radiation induced traps and the device readout scheme and clocking rates that determine the CTE behavior of an irradiated CCD [Mohs74].

To understand this interplay, we consider the readout procedure for a 2-dimensional CCD array. Signal charge packets are stored in the depletion regions formed underneath a biased gate during the integration period. Since the gate voltage determines the potential well capacity underneath, the signal charge can be moved down the rows in the buried channel by the appropriate sequencing of the gate voltages as indicated in figure 1. The charge is confined laterally to a single row by an implanted channel stop. After each "parallel" transfer of the charge from one pixel to the next, the charge packet is clocked out of the serial register, and the whole process repeated until the imager readout is complete. Signal electrons are captured very quickly by empty traps (~1 μs), but unfortunately the trap emission times are on the order of the time to read out the serial register. Hence, the signal charge can subsequently be re-emitted into a trailing pixel thereby degrading the CTE. Since the carrier emission times depend exponentially on temperature, the CTE response of a 2-dimensional CCD array is a strongly temperature dependent. In contrast to the typical area array, the linear CCD with clocking speeds at 1 MHz or more is relatively immune to proton induced CTE degradation. This is because the capture times for key radiation induced defect levels, such as the E-center, are too long relative to the charge transfer rate for the traps to efficiently trap signal charge. In general, we note that CTE degradation has a strong dependence on background signal level, clocking rate (dwell time within a pixel) and temperature as well as on the signal size. For example, figure 2 shows the charge transfer inefficiency (CTI = 1-CTE) as a function of background signal level, signal level and distance from the readout amplifier for a star tracker application. Such applications tend to near room temperature operation at high clocking rates. The results clearly show how application dependent the CTE truly is. Efforts have been made to predict CTE behavior in certain applications [Gall98], [Phil02] but this is still a difficult problem that will be discussed in the section on CTE measurements.
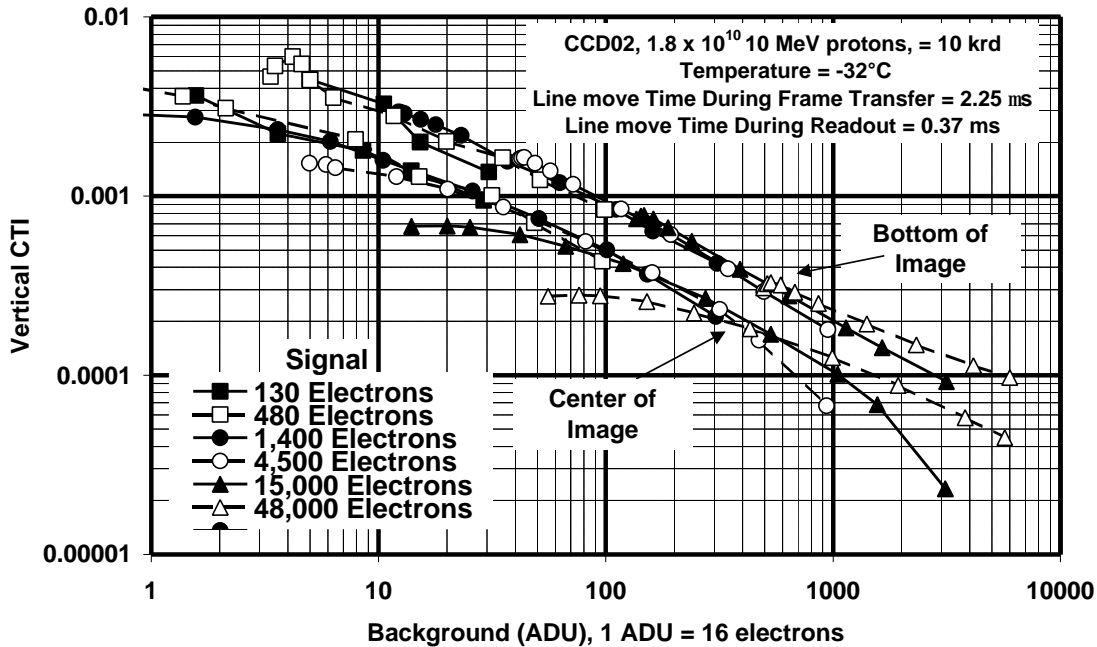
0.01

0.001

Vertical CTI

0.0001

0.00001

CCD02, 1.8 x 10^{10} 10 MeV protons, = 10 krd
Temperature = -32°C
Line move Time During Frame Transfer = 2.25 ms
Line move Time During Readout = 0.37 ms

Bottom of Image

Center of Image

Signal
■ 130 Electrons
□ 480 Electrons
● 1,400 Electrons
○ 4,500 Electrons
▲ 15,000 Electrons
△ 48,000 Electrons

1   10   100   1000   10000

Background (ADU), 1 ADU = 16 electrons

Figure 2. Vertical CTI at -32°C for an E2V CCD02 with pixel size 22.5x22.5 µm (including channel stops). From [Hopk00]. Note that the CTI is worse for the bottom of the image which is furthest away from the readout amplifier. Also the CTI improves with increasing background since the traps are kept filled. The dependence of CTI of signal level also varies with the location in the image.

Using typical values for the expected radiation-induced trap properties of these defects the CTI as a function of temperature can be estimated for the case of well-defined signal charges (e.g. 1230 electrons for Ti x-rays) and well separated (e.g. 220 pixels per x-ray event) as shown in Figure 3. Note that the trap activation energies appear in an exponential so that such a priori predictions are prone to error and the results are best used to understand overall trends. In many cases, the radiation induced defect of prime concern with respect to CTE loss is the E-center[4] (or phosphorus-vacancy defect), although the A-center (or oxygen-vacancy defect) can be important at very low temperatures [Bang91]. The improved CTE as one lowers the temperature to about -80°C occurs because the E-center traps remain filled as the serial register is read out so that there is reduced charge smearing. It is worth noting that the annealing temperatures for both the proton-induced A-center and E-center are at or above 150°C so heating of the device is not a practical solution to the CTE degradation problem. In the case of the Chandra CCD, the CTE became worse once the CCD was warmed to ambient temperature [Prig00]. We note that this is a high resistivity CCD for x-ray detection, and that it is not as yet clear what defect is responsible for this unusual behavior.

---

[4] For example, annealing measurements have shown that ~80% of the CTE degradation can be attributed to the E-center. See A.D. Holland, "Annealing of proton-induced displacement damage in CCDs for space use," Inst. Phys. Conf. Ser. 121, pp. 33-40, 1991.
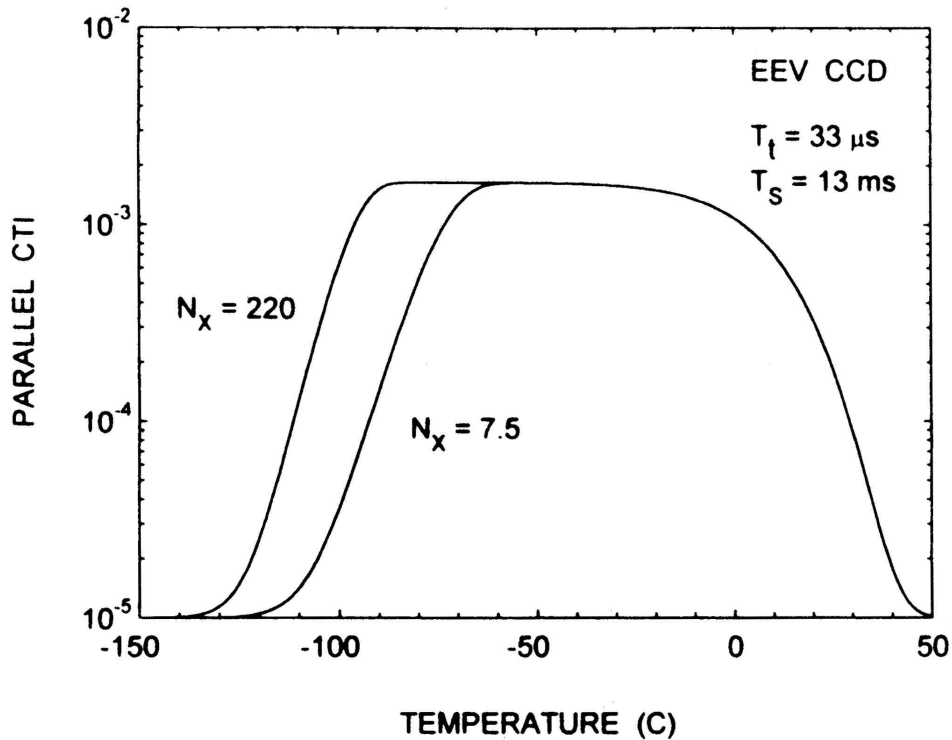
Figure 3 Shockley-Hall-Reed simulation of the parallel CTE loss in an E2V CCD showing the signature of the E center for two different x-ray intensities. [Dale93]

During the 1990s many groups were involved in studying radiation effects in CCDs for astronomical missions. As compared to many earth observing missions, astronomy observations are often made against a dark background and can involve low signal levels which are both challenging from a CTE perspective. Work for the Chandra [Prig00], XMM-Newton [Holm96], ASCA [Yama97] and Hubble Space Telescope (HST) [Holt95], [Wacz01], [Kimb00] programs showed that proton-induced CTE degradation (and hence detector sensitivity) can be very important, particularly at low signal levels. Unfortunately this can mean that key scientific observations become degraded first and therefore careful scheduling of the various on-orbit observations is important. In particular, faint objects will be increasingly lost in the noise as the number of parallel shifts increases.   Both the smallest observable amplitude and the efficiency of discovering faint objects is compromised. In addition, the photometric accuracy varies across an irradiated CCD, being highest for stars and galaxies near the serial register. Finally, the resolution of an object in the column direction will also depend on the its magnitude and location relative to the serial register. It is for all these reasons that the Advanced Camera for Surveys on board HST investigated the use of an optical preflash to fill radiation-induced traps ahead of data acquisition [Goli00]. The instrument is presently on-orbit, and has the ability to provide a post-flash (illumination after the

integration and before the readout) once the CTE degradation warrants it. For on-orbit CTE results from HST, visit the Space Telescope Science Institute's website (www.stsci.edu) that covers the HST 2002 Calibration Workshop.
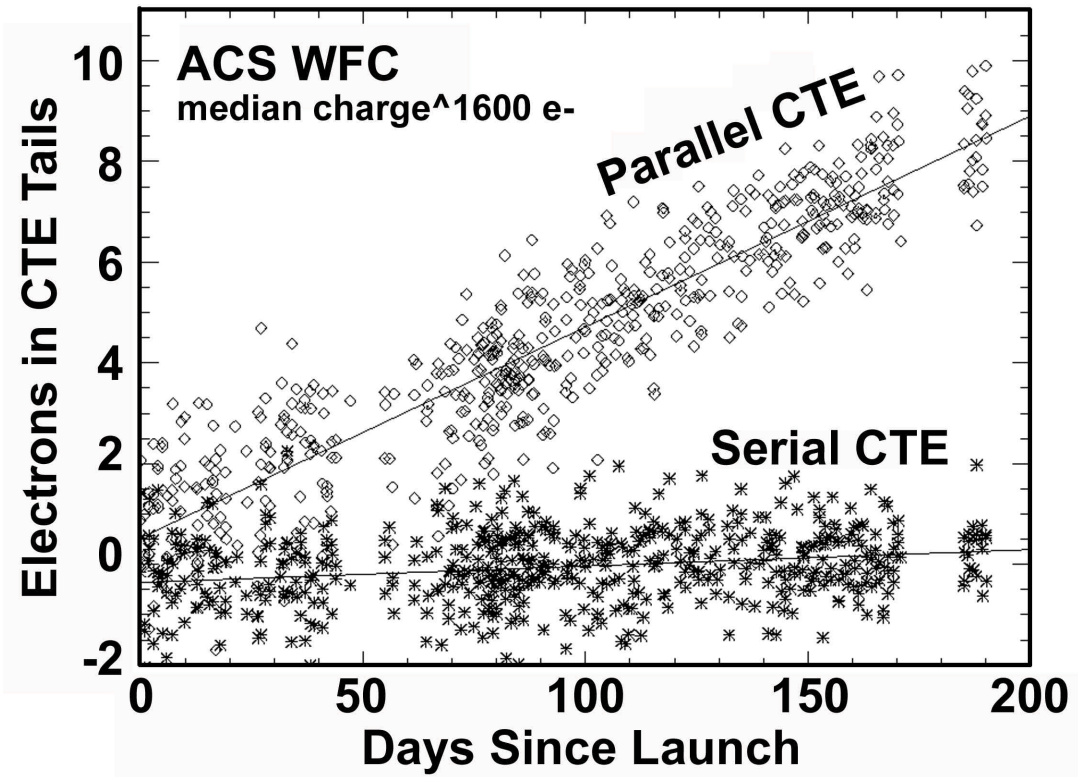

Figure 4 Advanced Camera for Surveys (ACS) Wide Field Camera (WFC) is showing significant CTE degradation as measured using cosmic ray tails. From [Reis02]. In another HST instrument (the Wide Field Camera 2 (WFC2)), the CTE has decreased 15 – 40% from 1991-1999, depending on the sky background level [Whit02]. Note that HST is a heavily shielded low earth orbit (LEO) application.

II. B. *ii.* Mean Dark Current and Dark Current Nonuniformity

The second major effect of proton induced displacement damage on CCDs is the increase in dark current as a result of carrier generation in the bulk depletion region of the pixel. (This assumes that the CCD has a hardened oxide and/or else is run in inversion so that the surface dark current is suppressed.) The average dark current increase has been shown to correlate with the amount of displacement damage energy imparted to the Si lattice by incoming protons. Note that low energy protons are more damaging than high energy protons. Although the increase in the mean dark current with proton irradiation is important, the dark current nonuniformity is generally the biggest concern for CCD applications in space. This nonuniformity is inherent to the statistical nature of the collision kinematics producing the displacement damage and therefore cannot be

hardened against. Incoming protons of the same energy may produce very different amounts of displacement damage depending on the particular collision sequence that follows as illustrated in figure 5. Very large dark current pixels can be produced when a collision occurs in a high electric field region (e.g. $> 10^5$ volts/cm)of a pixel as a result of electric field enhanced emission. (See reference 5 and references therein for more details.)
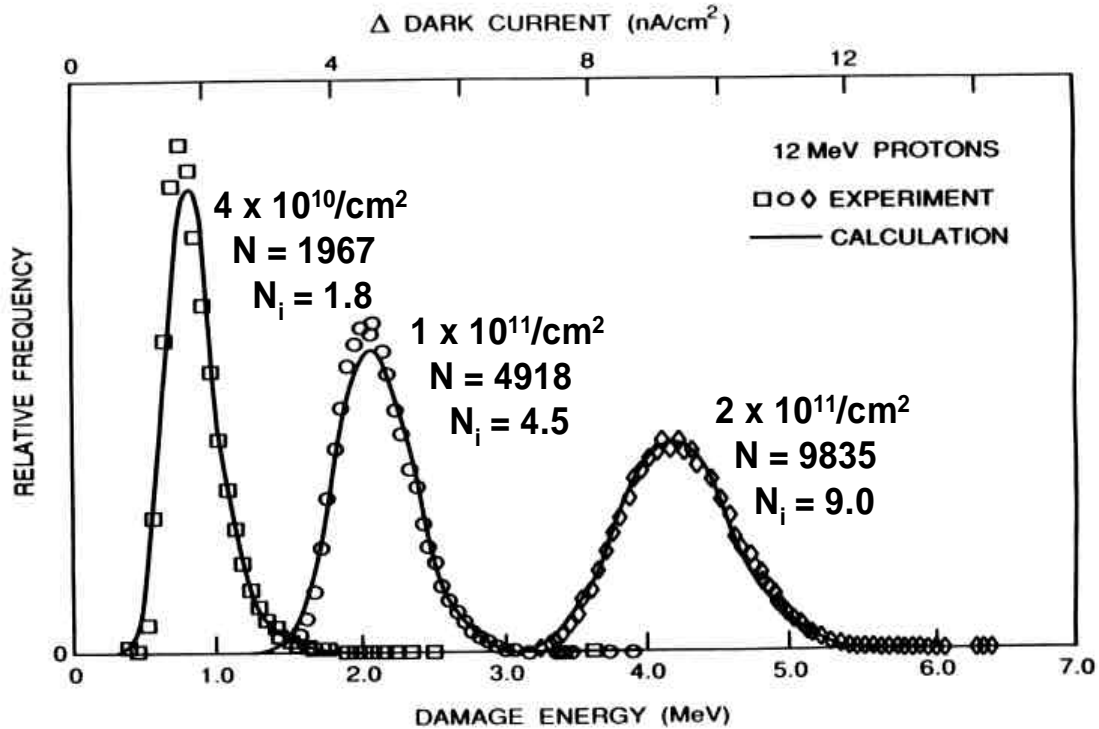

Figure 5 Charge Injection Device (CID) dark current histograms after exposure of a 256x256 array to increasing proton fluences. As the number of primary proton-Si interactions per pixel, N, increases the distribution approaches a gaussian distribution. The high energy tail is produced by very infrequent but large nuclear reaction events. (N_i is the average number of inelastic interactions per pixel.) After [Mars90] and [Dale89]. Such dark current nonuniformities are observed for any array of identical pixels whether it be a CID, CCD or APS device.

High dark current pixels (so-called hot pixels or hot spikes) accumulate as a function of time on orbit and present a serious problem for some missions. For example, the HST ACS/WFC instrument performs monthly anneals despite the loss of observational time, in order to partially anneal the hot pixels as demonstrated in figure 6. A very detailed study of the hot pixels in the HST Wide Field Camera 3 (WFC3) CCD has been performed [Poli03]. Note that the fact that significant annealing occurs for room temperature anneals is not presently understood since none of the commonly expected defects in Si (e.g. divacancy, E center, and A-center) anneal at such a low temperature.
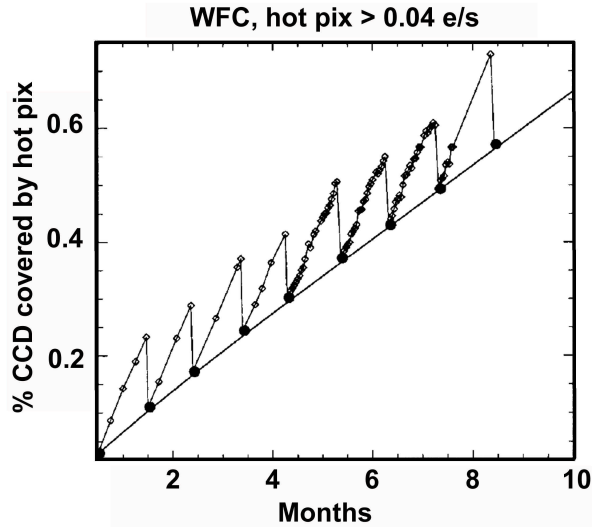
WFC, hot pix > 0.04 e/s

Figure 6   Hot pixel growth rates require monthly anneals that consume 10% of the observing time on the HST instruments (STIS, WFC2, ACS). From [Clam02].

II. B. *iii.* Random Telegraph Signals (RTS)

It has been discovered that some pixels in post-irradiated CCDs show a dark current that is not stable in time but switches between well-defined levels as indicated in figure 7 [Hopk93], [Hopk95]. These fluctuations have the characteristics of random telegraph signal (RTS) noise. This behavior is illustrated in figure 7 for an EEV CCD irradiated by 10 MeV protons. This type of noise has been observed on-orbit as well and represents a significant calibration problem for some applications.

EEV CCD05, 10 MeV Protons
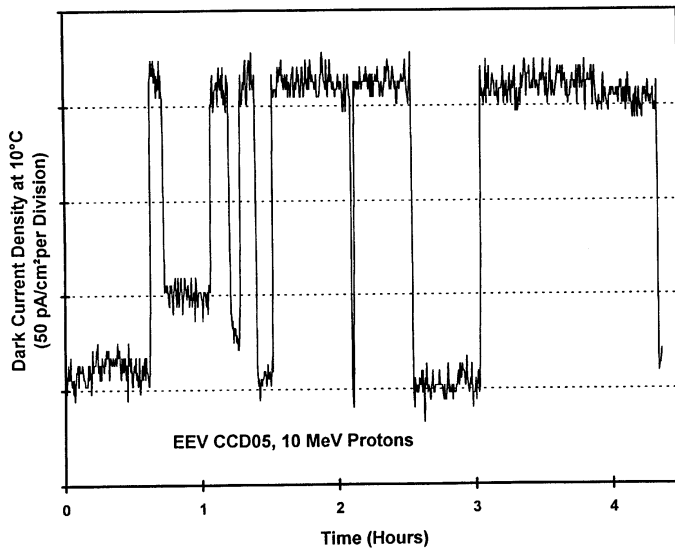
Figure 7   These RTS measurements were performed on an EEV imager at 10°C. The mean time constants for the high and low states increased at lower temperatures. After [Hopk93]. Usually only a small fraction of pixels show large fluctuations, but many show low level changes and these have to be taken into account whenever dark signal non-uniformity is important for an application.

13

II. C. Transient Effects

Transient radiation effects are produced when a particle (e.g. cosmic ray or trapped proton) traverse the active volume of a CCD. Ionization induces charge generation along the entire path of the incoming particle and produces a track that may cross multiple pixels as illustrated in figure 8. These events are transient since the charge produced is clocked out during readout. Nevertheless these transient effects produce significant noise in the readout and such events must be rejected to make use of the data acquired.

There are two techniques to minimize the effects from unwanted particle strikes. Imaging arrays on the NASA HST mission are troubled with these stray signals when in the South Atlantic Anomaly so much that they curtail the science operations when passing through this high flux region. When stopping operation is not practical, such as with a star tracker, transient events may be rejected by using a Kalman filter approach to average over several frames of imagery and reject signals which are not repeated in subsequent frames taken in view of the same region.

In figure 8, the four images have been acquired by a 1024 pixel by 1024 pixel CCD incorporated into one of the chronograph instruments on board the Solar and Heliospheric Observarory (SOHO) satellite. SOHO occupies an orbit around the L1 libration point. The coronagraph instrument filters the bright orb to focus on the details of the coronal structure; hence the dark circles in the center. The four panels depict the development of a coronal mass ejection (CME) on 11/6/97. The two lower panels show the effects of CME protons reaching the coronagraph's CCD. Even though the instrument has heavy shielding to protect the CCD, the > 100 MeV protons from the CME penetrated to the focal plane. Note the range of proton transient sizes and path trajectories indicating apparent omnidirectional arrival. Also note that the images are from different frames, and the proton transients are not repeated in the same image locations. For this reason, temporal filtering techniques can minimize the interference from the proton strikes for star trackers and other applications requiring tracking of bright objects against a cluttered background.
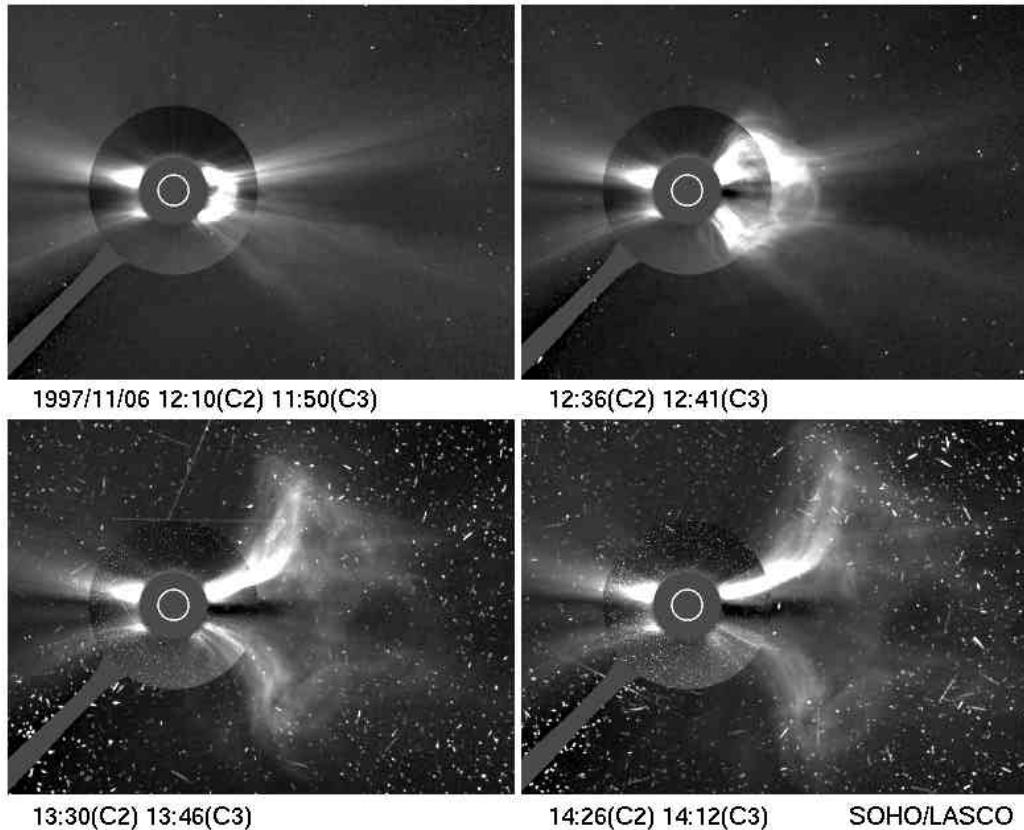
Figure 8. Coronagraphs from the SOHO satellite follow the evolution of a coronal mass ejection. Protons from the event reach the instrument's CCD and "pepper" the image with transients in the lower two panels.

III. CCD Measurement Techniques

In this section we will discuss various techniques used to measure CTE, dark current nonuniformity, and transient effects. CCD measurement techniques are described in great detail in reference 2. In the following chapter we will discuss CCD testing issues unique to the evaluation of the proton-induced CCD performance as evaluated during testing at a proton accelerator facility.

III. A. Assessment of CTE Effects

There are many techniques used to measure the CTE of a CCD, each with their own advantages and applicability to a particular situation. One popular method, due to it's inherent reproducibility, is the x-ray technique. X-rays are employed to produce well-defined and well separated charge packets which are read out and their intensity and location plotted. The technique will be described in more detail below but we note that the technique is capable of discerning very small changes in CTE, but is not appropriate to use in cases of severe CTE degradation. Signal charge packets may also be introduced electrically in some CCD designs [Mohs74]. Optical techniques include the use of bar

patterns, the extended edge pixel response (EPER), the first pixel response (FPR) and various other techniques involving spot illumination of a CCD. The EPER method employs a flat field illumination and overclocks the array to measure the deferred charge. In contrast, FPR measures the charge missing from the leading edge of a flat field image. A detailed comparison of the X-ray, EPER and FPR CTE measurement techniques can be found in [Wacz01].

Before describing CTE measurement in detail we note that the CTE is extremely application dependent. It is nontrivial to predict on-orbit CCD instrument performance based on a particular CTE measurement made on the ground. For example, scenes with a diffuse background charge provide some degree of "fat zero" that help to keep the radiation induced traps filled so that they do not remove charge from a signal packet. In contrast, astronomy missions may stare using long integration times to integrate sparse low level signals. In such a case, the radiation induced traps remove charge from the signal packets resulting in a reduction in CTE and the associated image smearing.   The CTE is also dependent on measurement conditions such as temperature, readout rate, clock overlap, signal level and CCD architecture.

III. A. *i*. X-ray CTE Measurement

The X-ray method provides an absolute measurement of CTE and also a precise gain calibration since the size of the signal charge packet is determined by the x-ray employed. For example, ^{55}Fe produces a 1620 e- packet whereas ^{109}Cd produces ~6,000 e- signal. Such measurements are easily compared between laboratories. As illustrated in figure 9, the CTE as measured by x-ray techniques is defined as

$$CTE_X = 1 - \frac{S_D(e^-)}{X(e^-)N_P} \qquad (1)$$

where SD(e-) is the average deferred charge after NP pixels transfers and X(e-) is the x-ray signal. Both the parallel and serial CTE can be measured using x-ray methods. The signal size is limited by the X-ray energy and packets of >6,000 electrons are not readily absorbed into a single pixel so other techniques are employed for large signal CTE measurements. Figure 10 illustrates the experimental stacked line trace obtained during an x-ray measurement. It is important to control the density of x-ray events since the CTE is dependent on the interplay of the mean time between clocked charge packets and the emission time constant of the radiation induced traps. Also, as shown in figure 11, the temperature dependence of the CTE also depends on the x-ray event density.
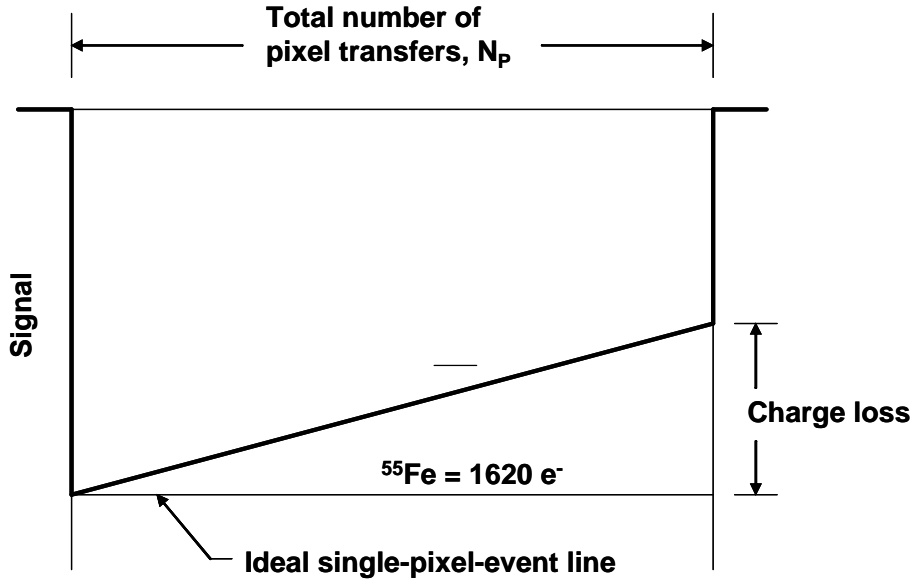
Figure 9 CTE measurement using x-ray signal charge packets.
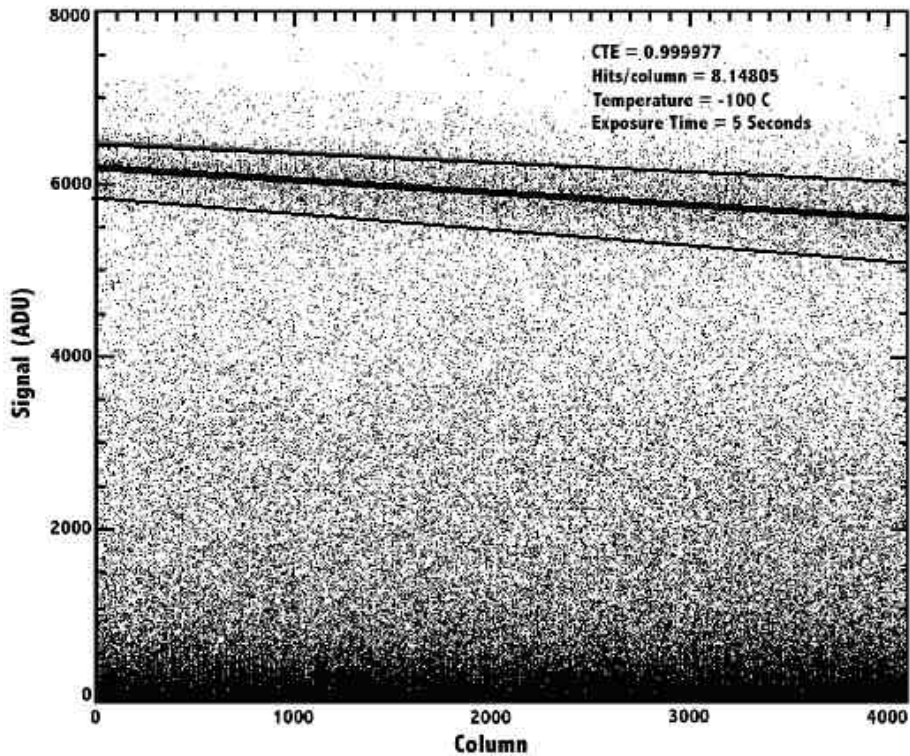

Figure 10 Stacking plot of post-irradiated ^{55}Fe data, with the upper and lower bounds of the K-alpha band, and the linear best fit to that area. Obtaining the slope of the best fit line and dividing it by the number of electrons/photon (1620 for ^{55}Fe) is the primary method used to calculate CTE from the ^{55}Fe images. X-ray density is directly related to the exposure time.
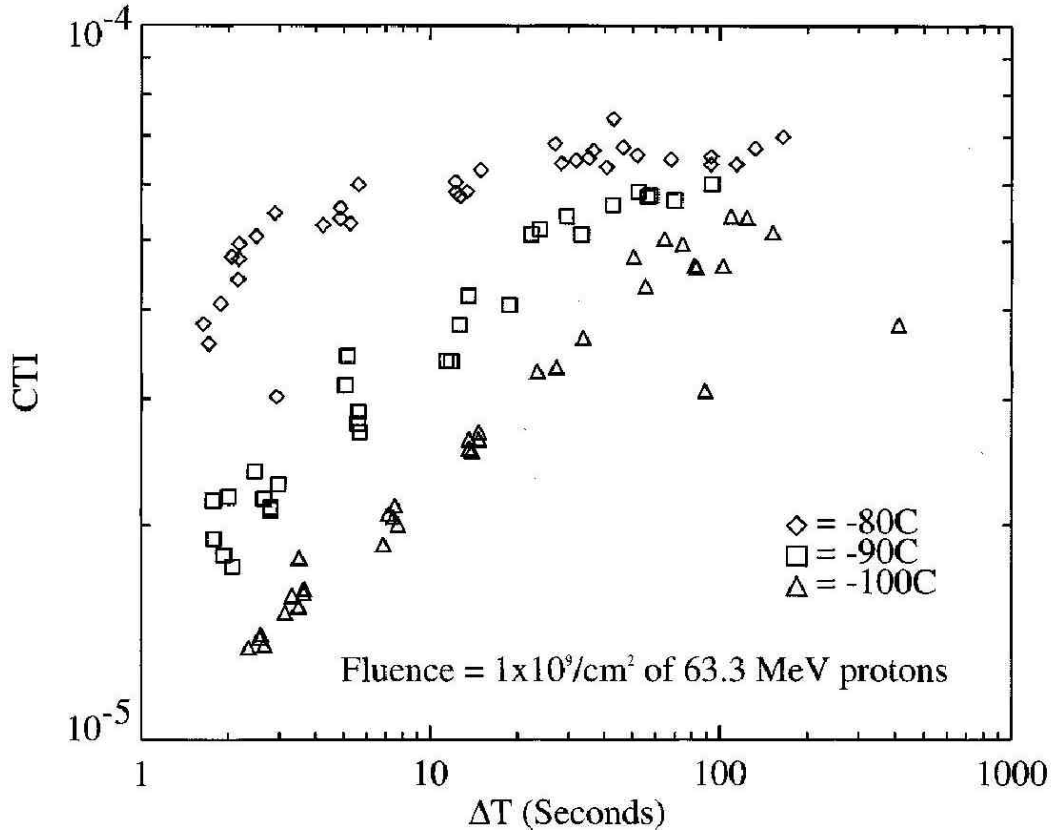
Figure 11   The charge transfer inefficiency (CTI = 1-CTE) versus the time between x-ray events (ΔT). CTE for images of medium density is a strong function of temperature whereas sparsely populated images are almost independent of temperature.

The x-ray technique does have limitations. In the case of very high performance CCDs the CTE can be so good that the tilt on the single event line is not measurable for the available number of parallel or serial transfers. In this case, there are related techniques described in [Jane01] whereby the charge is clocked back and forth to increase the number of pixel transfers in order to measure the CTE. Finally, we note that the technique is only viable when the dark current integrated during the x-ray exposure is small as compared to the x-ray signal. For radiation damaged CCDs, one typically cools the imager during the CTE measurement. Also, the technique works best with CCDs that have a thin epitaxial layer in order to obtain good 'single pixel' x-ray events. (A large field-free region below the depletion region leads to significant charge diffusion between pixels.) Note that the x-ray CTE measurement represents a worse case measurement for many applications (though perhaps not for some astronomical scenes) as a result of the small signal size and very low background.

III. A. *ii.* Extended Edge Pixel Response (EPER) Technique

The EPER measurement used a flat field illumination, and estimated the amount of deferred charge found in either the parallel or serial extended pixel region by overclocking the charge. Typically a number of lines are averaged together to improve

the signal-to-noise ratio in the extended pixel region. As described in [Jane01] and figure 12, the CTE from an EPER plot is defined as

$$CTE_{EPER} = 1 - \frac{S_D(e^-)}{S_{LC}(e^-)N_P}$$ (2)

where S_D is the total deferred charge measured in the extended pixel region. S_{LC} is the charge level of the last column, and N_P is the number of pixel transfers for the CCD register. The last column is specified because it collects diffusion charge from the neutral material surrounding the CCD during the flat field exposure. For example, if one calculates the CTE using the total amount of charge in 35 extended pixels in equation 2, the resulting CTE will be equivalent to that experienced by an isolated signal in a dark field, which is separated from the preceding signal by 35 pixels. As noted in [Jane01] and [Wacz01], care must be taken that all of the deferred charge is measured to avoid overestimating the actual CTE. If the clocking rate is too rapid, the deferred charge may spread out over many pixels and become lost in the read noise floor. This can occur since the charge is emitted from the radiation induced traps at a fixed rate whereas the time for transfer decreases as the readout rate is increased. Since the trap emission rate is very temperature dependent, the CTE as measured by EPER can vary as a function of temperature even for the same readout rate, as illustrated in the work of Waczynski et al. [Wacz01]. Note that when long emission time constants are encountered, released charge may spread over many pixels, and even beyond the practical overscan. A small amount of charge per pixel makes it difficult to recover from the noise. In this case EPER provides an overly optimistic CTE value. As with the x-ray techniques, many pixel transfers are required to get a readily measured CTE value. The EPER technique requires no special equipment and is capable of measuring CTE over a wide range of values. Indeed, it can be monitored during space missions since it simply requires a flat field exposure.
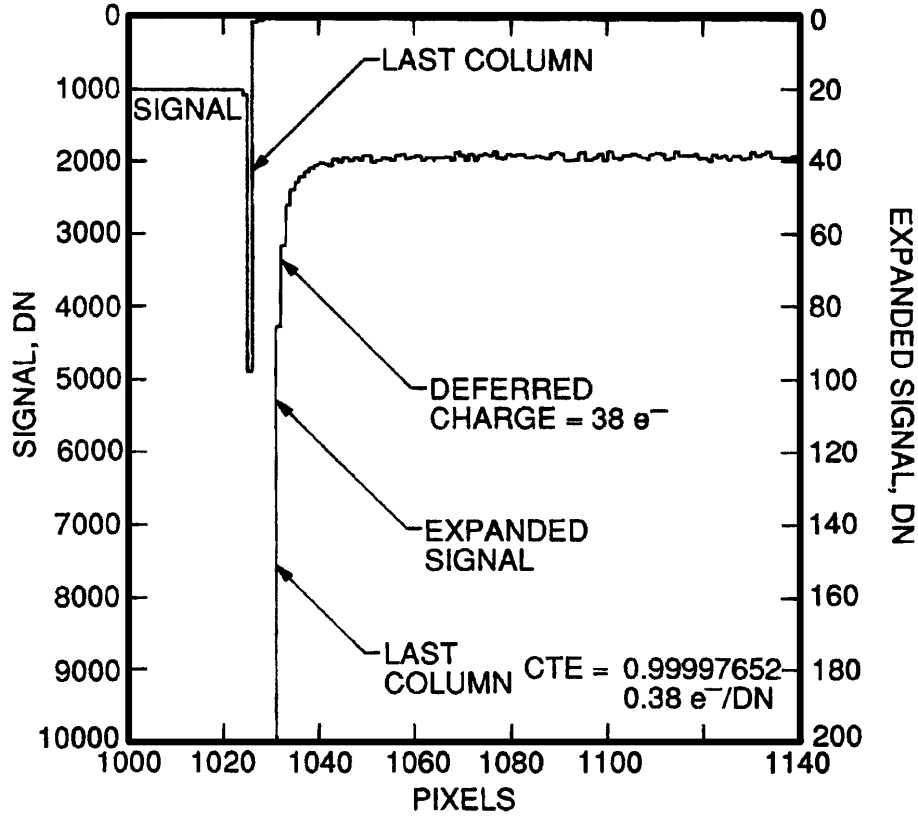
Figure 12 Horizontal (i.e. serial) EPER showing 38 e- of deferred charge after 1024 transfers in the CCD serial register. The noise in the extended pixel region was reduced from 6 e- to 0.15 e- by averaging 1500 lines of data. Adapted from [Jane01] p. 424].

III. A. *iii.* First Pixel Edge Response (FPR) technique

The FPR technique is similar to EPER, but measures the charge missing from the leading edge of a flat field image [Greg93]. Traditional FPR requires a frame transfer architecture wherein the parallel (vertical) and serial (horizontal) registers of the CCD are split and independently clocked. As described in [Jane01], to make a parallel CTE measurement using FPR, the CCD is exposed to a flat field illumination and then the storage region is readout (erased) several times. Then the image region is read out through the storage region. The first lines read through the empty storage array will lose charge to the radiation induced traps present. The total lost charge, S_D, is measured for a given number of pixel transfers, N_P, and the CTE determined from

$$CTE_{FPR} = 1 - \frac{S_D(e^-)}{S(e^-)N_P}$$
(3)

where S is the average charge level. Note that it is important to obtain the total charge lost from the first several lines read out and not just the first pixel, especially for low

signal levels and poor CTE conditions [Wacz01]. Similarly, the FPR method may be used to determine the serial CTE in devices with a split serial register.

As discussed in [Hopk99 and Hopk01], electronic injection and varied clocking techniques may also be employed to perform FPR measurements in such a manner that the signal and background levels can be independently varied to allow the assessment of the CTE under a variety of conditions. FPR provides a quick and accurate means of characterizing the CTE as a function of integration time, signal level, background level and temperature. This flexibility permits the CTE measurement to be designed to more closely approximate a given application. For example, during many missions the CCD may be detecting significant background charge and/or varied signal strengths. In such cases the traditional FPR measurement with no background signal would represent a worse case CTE measurement for a given signal size. This is because a diffuse background charge helps to keep the radiation induced traps filled so that they do not remove charge from a signal packet.   Finally, FPR may also be used to measure the emission time of the radiation-induced traps which can be useful for predicting the CTE response as a function of temperature and readout rate [Hopk1999, Hopk2001].

III. A. *iv.* Spot Illumination Measurements of CTE

In contrast with astronomical application that tend towards low temperature operation with low image backgrounds, long integration times and slow readout rates, star trackers and remote sensing instruments typically operate near room temperature with higher readout rates. Note that higher temperature operation results in higher dark charge generation ('fat zero') that helps to keep the radiation-induced traps filled. Of course this also means that the application must involve large enough signals relative to the background. Hopkins et al. describe an optical technique wherein they project green light onto a 12.5 μm pinhole [Hopk94].   After integrating light from the spot illumination, the charge is frame-transferred into the CCD storage region which is shielded from the light. At that point various transfer sequences were carried out in order to measure the emission time constant of the dominate CTE defect and the effects on CTE of radiation exposure, temperature, signal size and clock waveform. The reader is referred to [Hopk94] for further details of this CTE measurement technique.

In the case of a star tracker application one is often interested in assessing the centroiding accuracy as a function of radiation-induced damage. The effect of CTE degradation on artificial star images can be assessed as described in [Hopk00].

III. B. Assessment of Dark Current Nonuniformity

As described earlier, dark current nonuniformity always exists as a result of the statistics associated with the collision kinematics as the incoming proton interacts with the Si lattice. The dark current nonuniformity can characterized by analysis of full frame

data acquired using correlated double sampling.[5] A pixel by pixel subtraction of the dark frames before and after irradiation is used to generate dark current histograms such as the one shown in Figure 5.

Hot pixel populations can be further investigated using extreme value statistics as described in [Mars89] and [Mars90]. Extreme value statistics provides a simple method of determining if the hottest pixels present in a dark current histogram arise from a different physical mechanism such as electric field enhanced emission which has been found to result on very high dark current pixels in some devices. Measurements of the dark current activation energies of the hot pixels can also be used to assess whether electric field enhanced emission is the cause of high dark current pixels [Srou89]. Since hot pixel formation is very dependent on the electric field in the CCD, different technologies will have varying susceptibilities to hot pixel generation.

The formation and annealing of hot pixels in CCDs was studied in detail by Polidan et al. [Poli03] in preparation for the HST Wide Field Camera 3 (WFC3) deployment. Several HST instruments have experienced such an accumulation of hot pixels as a function of time on orbit that a monthly anneal at about room temperature is required to achieve a partial annealing of the hot pixels. Polidan et al. measured the introduction rate of hot pixels and their statistics, hot pixel annealing as a function of temperature and time, and the radiation-induced change to the mean dark current.

Polidan et al. note that the hot pixel population must be precisely defined. For example, HST Advanced Camera for Surveys (ACS) reported a prelaunch mean dark current of 9.25 +/- 1.02 e^-/pixel/hr based on 4 1000 s frames. They used 12 times the average standard deviation of the dark distribution, or 144 e^-/pixel/hr as the threshold for hot pixel formation. In contrast the WFC3 E2V CCD43s have <0.1 e^-/pixel/hr dark currents at -83°C and the ACS threshold criteria would lead to a WFC3 threshold of only 13.5 e^-/pixel/hr. Since the readout noise on the WFC3 CCD is 3 e- and the threshold should be significantly higher than 5 sigma to avoid false positive, the WFC3 team used fixed rates to define the hot pixel thresholds. The WFC3 dark current requirement is <20 e^- at -83°C , so hot pixel thresholds of 20, 40, 80, 160 and 144 e^-/pixel/hr were studied. For the room temperature portion of this study, the hot pixel threshold was defined as the mean plus 5, 10, or 15 times the standard deviation

---

[5] Double correlated sampling is used to optimize the signal to noise in the output. For details see p. 557 in [Jane01].

III. C. Assessment of Transient Effects

    Heavy ion and proton transient effects such as charge spreading may be assessed by acquiring sparse hit frames. The incoming particle flux is reduced so that there are many fewer than one strike per pixel during the integration and readout times of a particular device so that individual transients can be studied [Srou86], [Lomh90], [Mars02]. A series of dark frames are acquired prior to exposure to the beam to provide a baseline to subtract out all effects save the transients themselves.

IV. Application Specific Nature of CTE

    CCDs are used in a wide variety of applications. Astronomers may integrate for 1.5 hours and readout slowly at temperature down to -110 °C, whereas a star tracker may require high speed operation at near room temperature. Imaging applications may view high or low background levels. The causes of CTI and its dependence on particular irradiation induced defects, imager geometry and readout conditions (e.g. temperature, readout rates and modes, clock overlap, etc.), can explored using Shockley-Hall-Reed theory for the case of x-ray CTE measurements [e.g. Jane01, Dale93, Hopk94, Mohs74]. Such analysis (as exhibited in Figure 3) clearly shows that CTE loss can be somewhat reduced by substantial cooling (often to about –80 °C or lower), to mitigate the trapping effects of the E-center (and also minimize dark current).   We note that x-ray CTE measurements, though important for studying basic mechanisms and evaluating high performance CCDs, do generally represent a worst case. During many missions, CCDs will be detecting significant background charge and/or larger signals. Many scenes produce a diffuse background charge that provides some degree of "fat zero" that help to keep the radiation induced traps filled so that they do not remove charge from a signal packet. Also, larger signal sizes occupy less volume per electron, which is observed to improve the CTE [Mohs74, Jane91, Hard98] with increasing signal size. As illustrated in figure 13, background charge can dramatically impact the CTE loss by filling the traps so that they do not interact with the signal charge packet.   The magnitude of the improvement depends on the signal size, and usually (though not always [Robb92]) comes at the price of additional noise.
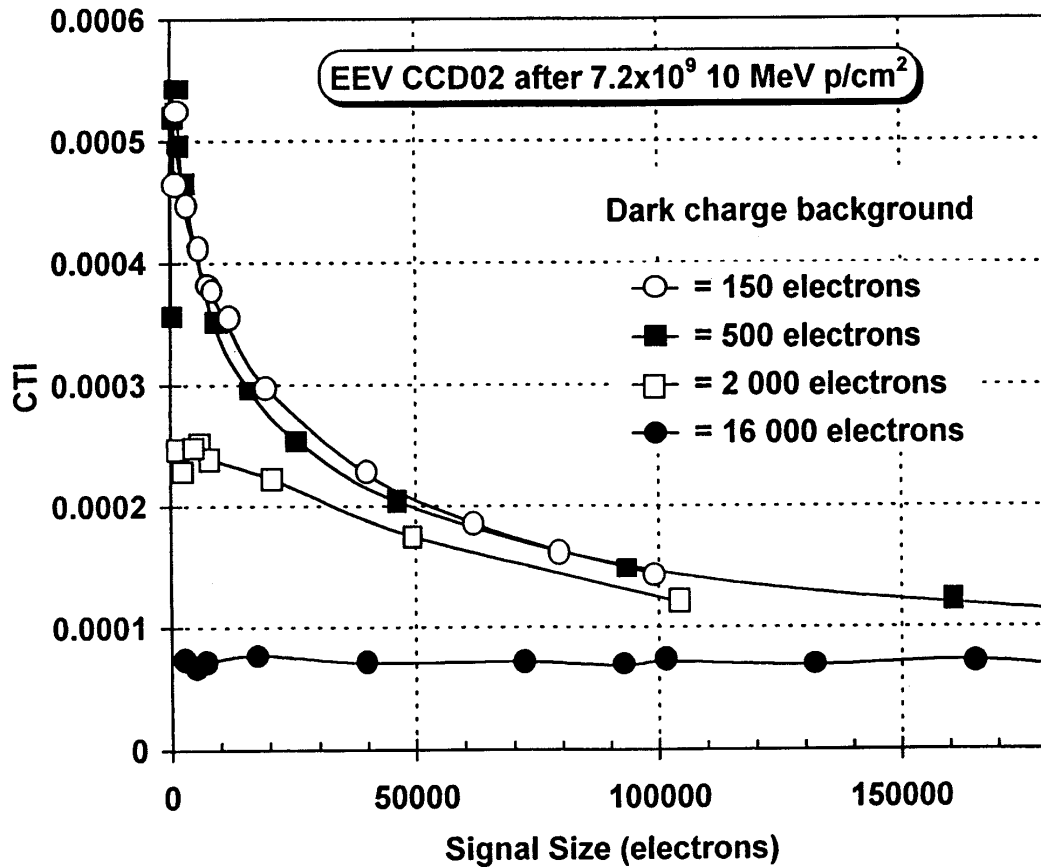
Figure 13 The charge transfer inefficiency (CTI = 1-CTE) for a CCD exposed to a proton fluence of 7.2×10^9 cm^{-2}, corresponding to TID of 4 krad(Si). Both the CTI and the efficacy of a dark charge background in CTI reduction are a function of signal size. After [Hopk94].

It is important that the CTE measurement employed for a given mission either faithfully reproduce the expected conditions (generally not practical) or provide a worse case measurement. In the case of star tracker applications one may measure the centroiding accuracy of an irradiated CCD using a relevant simulated star scene. If this is not possible then the pinhole and near room temperature techniques in [Hopk94] may be applicable. For astronomy applications, techniques including x-ray, EPER or FPR may be more appropriate. One of the biggest challenges facing the CCD radiation effects engineer is to identify a laboratory radiation test that provides an accurate indication of the on-orbit performance expected for a device or subsystem.

IV. A. CTE at Low Operating Temperatures (ESA GAIA Case Study [Hopk01])

A recent paper by G.R. Hopkinson [Hopk01] provides a good summary of CCD behavior at low temperatures of interest to many astronomy missions including HST, Chandra, XMM-Newton, GAIA, etc. The low temperature reduces the dark current to

near-negligible levels to enable very long integration times. Charge transfer efficiency improves since the trap emission times increase and therefore traps remain filled more easily (either by the signal or deliberately injected charge.) Hopkinson measured the CTE response as a function of signal level, temperature, background signal level using the FPR method. Figure 14 show the results for both low and high signal levels as a function of temperature. We see that the CTI is relatively insensitive to temperature for high signal levels and reaches a minimum at about -100 for low signal levels. The low signal CTI increases at higher temperatures due to the E center and at lower temperatures due to the A-center.
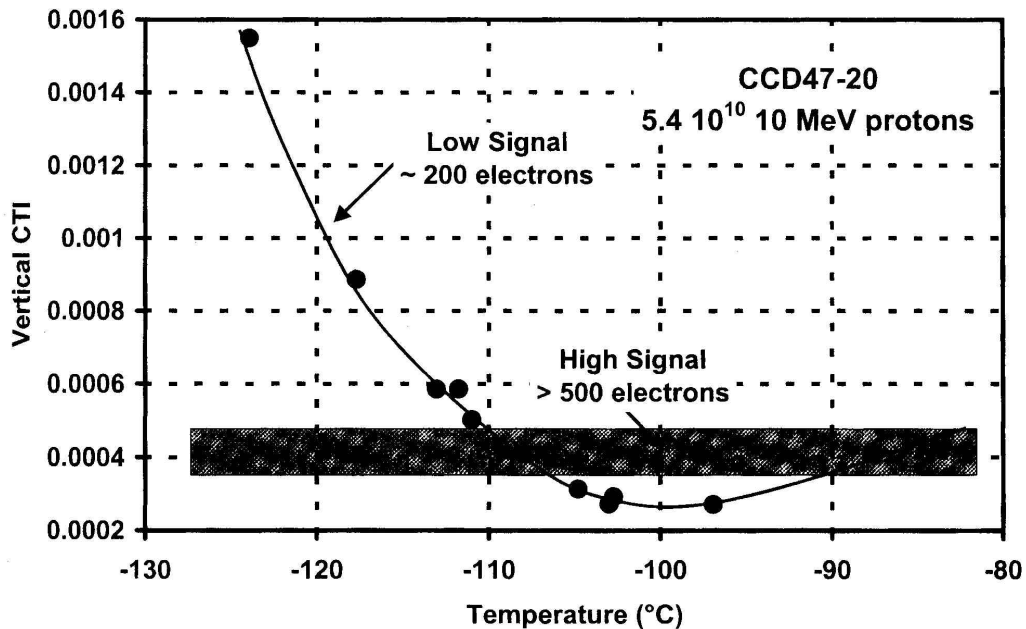
Figure 14. FPR measurements of the vertical CTI as a function of signal level for a Marconi CCD47-20 after exposure to 30 krad(Si) from 10 MeV protons for a background of ~10 electrons.

The GAIA mission is considering the use of large (near full well) preinjection LED pulses to mitigate CTI loss. The effect of the pre-flash are illustrated in figure 15 for a CCD exposed to 30 krad(Si) of 10 MeV protons. The brightest pre-flash produces the lowest CTI but there is a noise penalty which must be considered. The CTI also depends on the timing between the signal and charge injection as described in [Hopk01]. The LED preflash method of reducing the CTI has been considered by several missions including the Advanced Camera for Surveys (AC) on board HST. [the preflash is which HST instrument. Versus electrical preinjection ahead of signal? and Chandra [Prig00].

Figure 15 CTI as a function of temperature for a relatively high signal level and background with a preflash 290 ms ahead of the signal. When there is no flash, the preinjection level is the same as the signal level as a consequence of the FPR method.
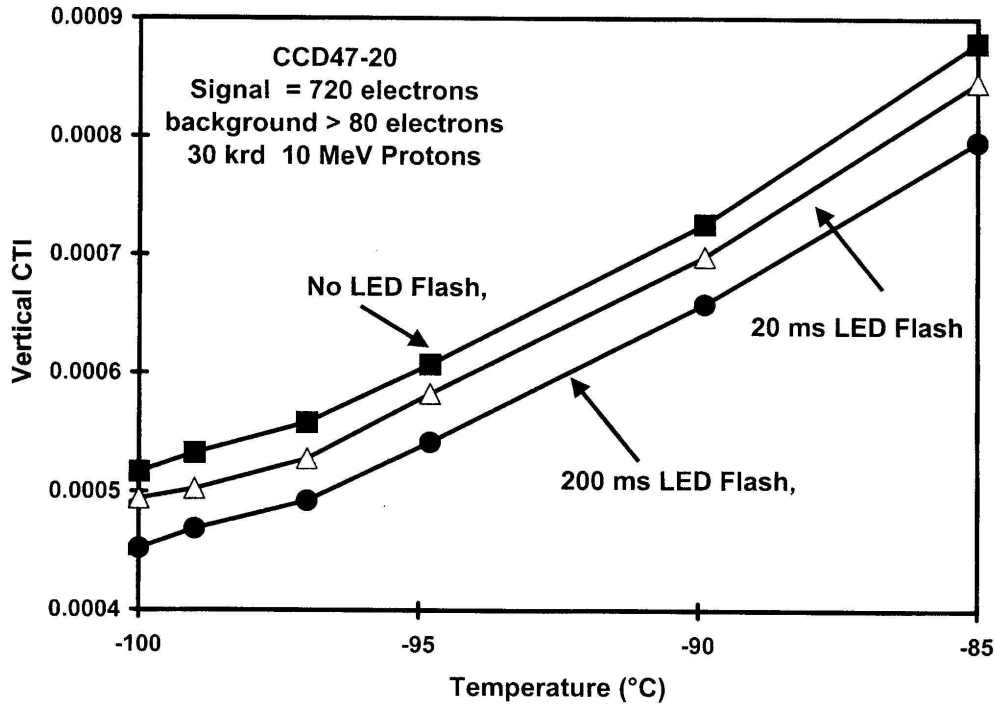
IV. B.   Comparison of CTE Measurement Techniques and CTE Noise   (HST WFC3 Case Study [John00 and Wacz01])

Waczynski et al. have performed a detailed CTE investigation on the Marconi CCD44 devices used on the WFC3 instrument [Wacz01]. The CCDs are back-illuminated and have a 4096 x 2048 format with 15 μm2 pixels and amplifiers at both ends of a single 2048 pixel serial register. The study included 63 MeV proton fluences up to 5 x109 cm-2. Significant degradation in the CTE was observed but no changes in the read noise were measured. The CTE was measured using three methods (EPER, FPR and [55]Fe). The x-ray methods are widely reported in the literature and provide an absolute CTE and are therefore very useful for laboratory-to-laboratory comparisons. However, heavily damage devices cannot be studied using [55]Fe and x-ray sources are only practical for signal sizes up to ~6,000 electrons so other photometric-based techniques are necessary. The EPER method is also widely used but can produce overly optimistic results as noted above. The FPR is a valuable CTE measurement technique when a frame store architecture permits it, and like [55]Fe provides an absolute measurement which is preferred especially for small signal levels.

The CTE value measured by the [55]Fe technique is very dependent on the x-ray density of the set-up especially at lower temperatures [e.g. Wacz01]. In addition, we note that the CTE for very sparse images (i.e. very low x-ray density) is essentially independent of temperature whereas for medium densities the CTE is a strong function of temperature. (Recall figure 11.) We cannot overstress the application-dependent nature of the CTE. Waczynski et al. found that the [55]Fe, EPER and FPR methods gave essentially the same CTE at -80°C, but at -90°C we see that the EPER measurement overestimates the CTE as can be seen in figure 16. This occurs because at colder temperatures it becomes more difficult to account for all the deferred charge given the limited overscan capability when employing the EPER technique.
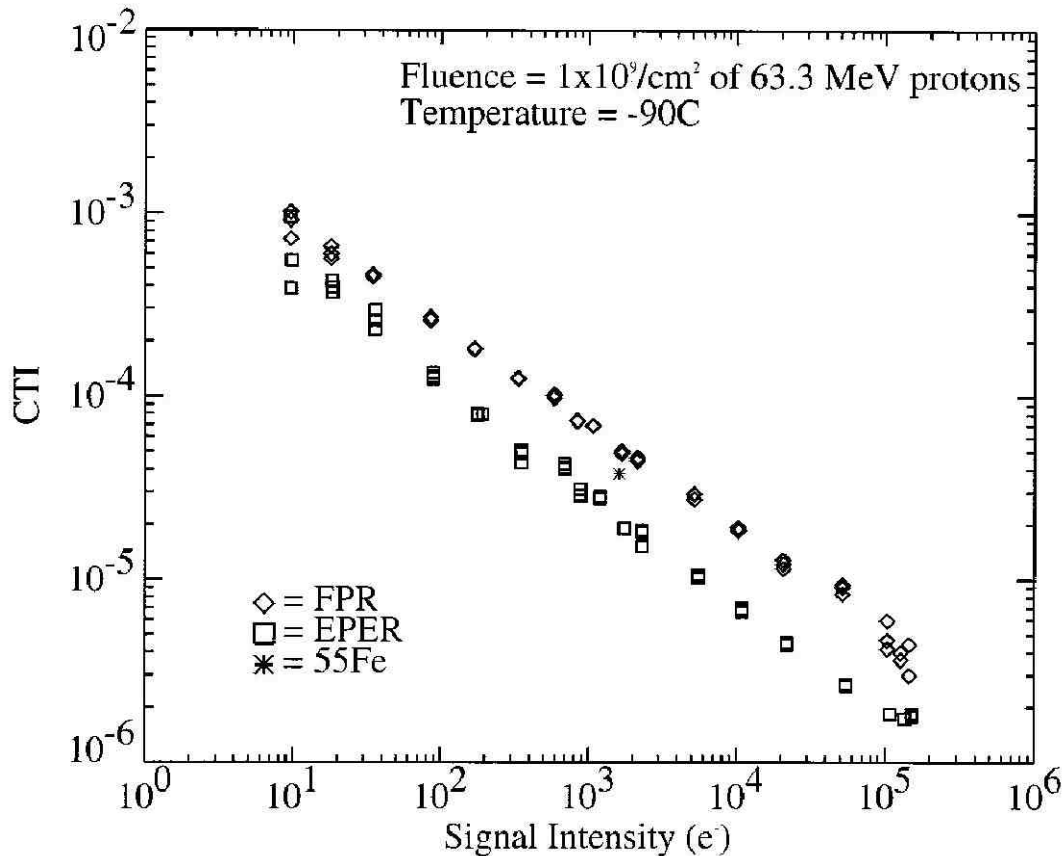
Figure 16   EPER overestimates the CTE at -90 C because the longer emission time constant means that charge is released over many pixels, and even beyond the practical overscan. Also, a small amount of charge per pixel makes it difficult to recover signal from the noise.

The amount of displacement damage and hence trap density varies from column-to-column and so one would expect the CTE to also be column dependent. This so-called 'CTE noise' was also characterized by Waczynski et al. and is a type of fixed pattern noise which could be corrected if it were understood well enough.

Finally, in this case study [Wacz01], the post radiation CTE of two CCDs were compared, one with and one without a notch, and no significant difference was found. It is commonly held that the notch would reduce the CTE degradation for low signal levels by confining the charge to a smaller volume, but we note that the improved performance has not been evident in several studies. Perhaps, there are specific readout conditions required to observe the advantage of the notch. Again, this proposed CTE hardening technique may be very application specific and must be demonstrated for your particular instrument.

CTE is a local phenomenon and can vary widely across a CCD. The statistical nature of CTE degradation was studied on flight-like Marconi CCD43s for the WFC3 project [John00]. In radiation-damaged CCDs, CTE noise can be the dominant source of noise. In contrast to other noise sources it has a component of fixed pattern noise that can be removed by the appropriate calibration technique.

V. Proton Ground Testing Issues

For any application where displacement damage is expected to produce significant degradation, it is important to perform a proton radiation test in addition to the routine Co-60 TID evaluation. In the case of CCD testing, the combination of limited device availability and time-consuming measurement procedures results in the use of proton irradiations to evaluate both the TID and displacement damage response of a device. Note that for proton energies above about 40 MeV, the proton-induced rad(Si) can be considered equivalent to a Co-60 rad(Si) [Mars99], and it is therefore straightforward to calculate the proton induced TID.

Protons occur in every imaginable orbit with variations in spectral energy composition, arrival rates, and sometimes arrival trajectories. The three sources are trapped protons in the inner Van Allen radiation belt, the proton component of solar particle events, and hydrogen nuclei from intergalactic cosmic rays. Careful discussions of the near-Earth, interplanetary, and other planet proton environment models are available in the NSREC Short Course notes from 1997 [Bart-97]. For the radiation effects engineer, detailed understandings of the environment models are fortunately not usually necessary. Instead, the proton and other radiation related requirements are either supplied by the procuring organization or generated "in house" by resident radiation environment experts. In order to design an appropriate proton ground test, it is essential to request the expected proton energy spectrum associated with the mission lifetime. Note that the environment provided should include a factor of two margin to account for the uncertainty in the derivation of the orbital environment, and may also include other design margins associated with uncertainties in on-orbit prediction techniques for a particular device. For example, the environment may be increased by as much as 50% to account for secondary production in a thick high Z shield surrounding a CCD. The environment information will permit the test engineer to determine the appropriate proton test energy and fluences.

V. A. Selection of Proton Test Energies

In order to convert the proton spectrum for a particular mission to an 'equivalent fluence' at a specific proton energy, we calculate the proton fluence at our test energy that will produce the same amount of displacement damage in the CCD as the spectrum of protons for the mission duration. It is possible to test at only one proton energy because of the existence of an approximate correlation between the calculated displacement damage energy function and the CCD performance as a function of energy. The displacement damage energy function is called the nonionizing energy loss rate (NIEL) and is described in Appendix A. Although multiple test energies may be desirable, program constraints often restrict proton testing to a single energy, and it is important to choose the test energy very carefully.

We will see that the choice of proton test energy will depend on the degree of device shielding in a particular application. Despite various mitigation approaches, for devices such as CCDs that are extremely sensitive to displacement damage, it is often necessary to resort to the use of thick shields to minimize the radiation damage at the CCD location. To illustrate the general trends observed for any orbit, we consider the following example. Figure 17 shows the integral displacement damage deposited as well as the corresponding CTE loss per year for the EEV imager in the 705 km, 97.4° polar orbit for four Al shield thicknesses. (The integral displacement damage dose and ΔCTE due to protons above a given energy are obtained by evaluating the integral from E to the highest proton energy.) The intercepts show the effects of particles of all energies in terms of non-ionizing energy deposited per gram Si per year, or as the ΔCTE per year. We see that the relative gains from adding shield mass diminish as the shield gets thicker. Also, except for lightly shielded imagers, most of the damage results from protons over 10 MeV. It can come as a surprise to discover that, in a heavily shielded application, half (or more) of the displacement damage dose is contributed by incident protons with energies in excess of 100 MeV. This is true despite the fact that lower energy protons produce more displacement damage, because the transported proton spectra are becoming much harder with increasing shield thickness. The spectral hardness occurs because the lower energy incident particles have a higher LET and are therefore preferentially stopped in the shielding.
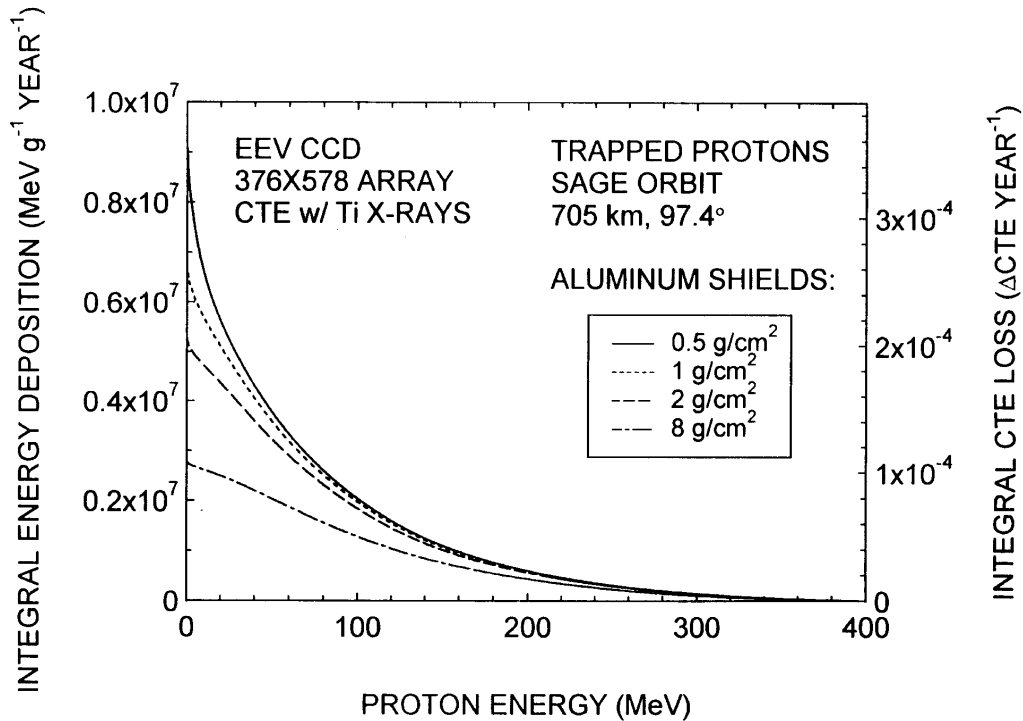
Figure 17 The integral damage spectrum (integrated from the energy in question to the highest proton energy) is shown versus proton energy. The intercepts at zero energy give the yearly total damage for the entire proton spectrum. The values in order of increasing shield thickness are 9.2×10^6, 6.7×10^6, 5.3×10^6, and 2.93×10^6 MeV g(Si)$^{-1}$ year^{-1}. The corresponding CTE losses per year given from the right ordinate are 3.6×10^{-4}, 2.6×10^{-4}, 2.0×10^{-4}, and 1.1×10^{-4}, respectively. After [Dale93].

Many of the space applications employing photonic devices (e.g., CCDs, etc.) are heavily shielded, and the peak in the transported proton spectra is shifted to higher energies, typically between 40-100 MeV. The optimal choice for a single test energy is the one that best represents the *damage-weighted* proton spectrum calculated using a displacement damage function. Hence, higher energy protons are frequently employed for radiation tests. For example at the proton cyclotron at the University of California at Davis, monoenergetic protons can be obtained up to an energy of about 63 MeV.[6] There is another reason for choosing higher proton energies. They penetrate CCD packaging and the device itself without significant energy loss which is highly desirable. Finally, we recall that we can best correlate Co-60 TID rad(Si) with the ionizing dose produced by protons with energies over 40 MeV. For all these reasons, monoenergetic proton energies between 40-63 MeV are typically used to assess displacement damage in CCDs.

---

[6] We strongly encourage the use of a tuned monoenergetic proton beam. It is not appropriate to use a significantly degraded proton beam for devices sensitive to displacement damage. Degraded beams have straggle in the proton beam energies which introduces significant uncertainty into the data analysis.

V. B. Calculation of Displacement Damage Equivalent Fluences

Once one or more proton test energies have been chosen for a particular space mission, the relevant MeV-equivalent fluences for a particular mission can be calculated using the calculated NIEL and the differential proton fluence spectrum, $d\Phi(E)/dE$, for the time period of interest. Note that a given mission may be represented by a time-weighted sum of more than one differential spectrum depending on the details of orbital precession, solar cycles, etc. The MeV-equivalent proton fluence at a given test energy, E_{test} is given by:

$$\Phi(E_{test}) = \frac{\int\limits_{E1}^{E2} \frac{d\Phi(E)}{dE} NIEL(E)dE}{NIEL(E_{test})} \qquad (4)$$

where the numerator is just the total displacement damage dose in units of MeV/g when NIEL(E) is expressed in units of MeVcm^2/g. The integration limits, E1 and E2, generally correspond to the lowest and highest proton energies provided in the differential spectrum, typically from about 0.01 MeV to about 500 MeV. Note that the range of integration may be reasonably adjusted depending on the degree of shielding present [Dale91].   As an example, a 60 MeV-equivalent fluence is simply the fluence of 60 MeV protons that produces the same amount of displacement damage dose as the time-integrated transported proton spectrum representing the mission environment.

Equation 4 can also be used to calculate the mission equivalent fluence at a proton energy for which there is relevant device data in the literature. In this way, one can assess the suitability of a candidate device for a particular mission, or (as often is the case) to provide an initial assessment of a device already chosen. For example, figure 18 shows the CTE degradation both as a function of years in orbit (HST) and equivalent 63 MeV proton fluence.
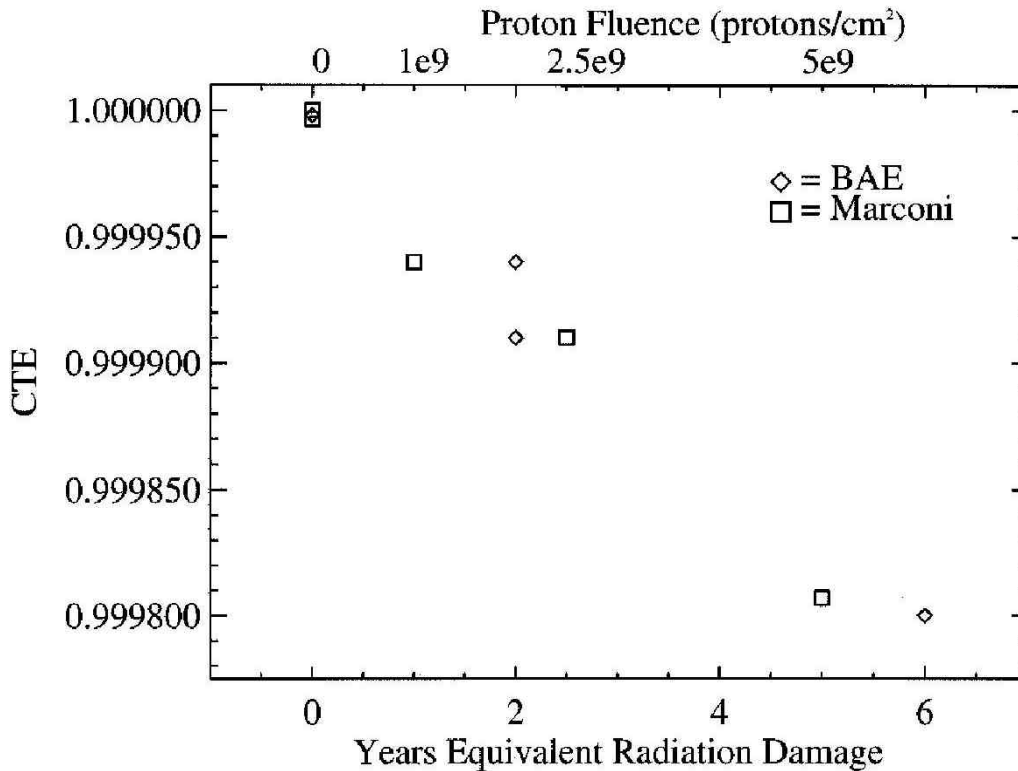
Figure 18 CTE as a function of proton fluence for 2 CCDs shown with equivalent time on orbit for HST.

V. C. Proton Test Plans

The large majority of proton test plans call for passive exposures with the detailed characterization occurring back at the laboratory. Often test plans are driven by the available number of devices and time constraints. The same device may be utilized to obtain data at multiple fluence levels if one has the time for multiple trips to the proton cyclotron. Since it is always recommended to acquire key data on a flight lot device, one typically designs the ground testing to utilize a minimum number of CCDs. If sufficient relevant devices are available, one uses several CCDs and samples a few key fluences such as one half, one and two times the mission equivalent fluence at the chosen test energy. Note that modern devices can be large relative to the uniform beam area, and it may be necessary to tilt the device relative to the beam. Proton test energies should be selected based on the particular application, as described earlier, but it is always important to ensure that the incident proton has sufficient range to penetrate both the device packaging and the sensitive volume of the device itself. The analysis is greatly facilitated (and more accurate) if the non-ionizing energy loss (NIEL) rate through the active volume of the device is constant, and if the incident proton beam is reasonably monoenergetic. As noted above, CCD applications are typically heavily shielded so that the mean energy of the shielded proton spectrum has increased to the 40-100 MeV range. At such high energies, the protons are very penetrating and the NIEL is constant throughout the CCD.

It is worthwhile noting that other proton energies are often used for proton testing. Much testing for the European Space Agency has been performed at 10 MeV because of the easier availability of this proton energy. One disadvantage of this energy is that it does not provide a representative sampling of the nonelastic proton-silicon interactions that are responsible for much of the observed pixel-to-pixel nonuniformity on orbit. For this reason, we continue to recommend testing at higher proton energies for heavily shielded missions. Finally, we note that the front-illuminated x-ray CCDs on board the Chandra Observatory experienced significant low energy proton exposure during passages through the SAA. This unexpected result was the consequence of low energy protons (~100-300 keV) scattering at low angles of incidence through the x-ray optics of the ACIS instrument and producing significant displacement damage in the active regions of the front illuminated CCDs. (Such low energy protons have a nonionizing energy loss rate that greatly exceeds that of protons in the tens of MeV range and are therefore very damaging.) Fortunately, Chandra has been able to avoid further damage to the CCDs by shuttering them during passage through the SAA. Other similar missions such as XMM-Newton have baselined the shuttering option to avoid damage from low energy protons.

Typically, CCDs for astronomical applications are irradiated with all leads grounded. Since CTE losses are produced by displacement damage, effects of bias during irradiation on CTE measurements are not expected, and have not been reported (e.g. [Hopk00]). Note that if the devices were irradiated to levels high enough to produce significant total ionizing dose response they would not be functional for many of the applications considered in this paper. Dark current increases are mitigated by cooling the CCD on orbit. Full characterization of the irradiated CCDs generally is carried out back at an organization's home laboratory and may not commence until a week or two after the irradiation is complete.

There are applications (e.g. Earth observing missions flying as high as possible for increased Earth coverage) with less demanding CTE constraints that may expect 10 krad(Si) or more of ionizing dose. In such cases it may be advisable to irradiate the devices under a worse case positive bias, and then assess the CCD functionality soon thereafter. A typical flatband voltage shift for a commercial off-the-shelf (COTS) CCD is 0.1 V/krd(Si) when biased and around one half to one third that value when unbiased during irradiation [Hopk92, Robb93, Hopk96]. In contrast, the radiation-induced increase in surface dark current may [Hopk91] or may not [Hopk92] be dependent upon the bias during irradiation. Note that during non-inverted operation, unbiased CCDs may exhibit a radiation-induced surface dark current and flatband shift that *increases* with time ("reverse annealing"). The reverse annealing is attributed to a slow buildup of interface states, and varies from manufacturer to manufacturer. Generally, a 24 hour bake at 100 °C is found to accelerate the annealing process which expedites program testing [e.g. Hopk91, Hopk92]. Nevertheless, Hopkinson notes in [Hopk91] that for one device type the high temperature anneal produced what seem to be an inordinately large increase in the dark current which they had not (at the time of the report) compared to identical devices annealed at room temperature. Reverse annealing would be expected to be minimized by CCD fabrication processes that isolate the signal channel from the

bird's beak region [e.g. Jane01]. Such devices are recommended for higher dose applications.

Transient tests are occasionally indicated and are performed in real time with the sample in the beam line. The data are collected under low proton flux conditions so that probabilities of multiple proton strikes in the same portion of the array are negligible. Data analysis requires considerable efforts to identify valid struck pixels versus either erratic pixels or normal pixels influenced by the background of random noise. As a result both the clear (without beam) and a series of beam "runs" are both required. The first step of a data analysis scheme involves "scrubbing" to remove aberrant pixels. In this step, each pixel position is interrogated over the entire series of data frames frames, and flagged for removal from the analysis if anywhere it exhibited readings that are saturated, consistently erratic, or otherwise aberrant across multiple frames. After scrubbing the data frames for both the clear condition and the proton run to exclude invalid pixel positions, the average clear value for each individual pixel is subtracted from the corresponding pixel position for each frame in the data run. The resulting scrubbed and background subtracted data cube is then analyzed. It is important to periodically obtain clear reference frames for subtraction from subsequent data frames.

In some cases, very involved 'live' testing is warranted. For example, Polidan et al. [Poli03] performed a series of tests to characterize the formation and annealing of hot pixels in CCDs in preparation for the HST WFC3 deployment. They measured the introduction rate of hot pixels and their statistics, hot pixel annealing as a function of temperature and time, and the radiation-induced change to the mean dark current. Note that this requires a specialized dewar that can operate with the device in the beam. Care must be taken to ensure that no light reaches the detector during dark exposures. In addition, the dewar must be designed to minimize radiation-induced activation. For more details of this detailed test plan see [Poli03].

VI. Summary

CCDs are very high performance devices utilized by NASA, DoD and commercially for imaging, spectroscopy, star tracking, etc. Unfortunately, the performance of CCDs is permanently degraded by total ionizing dose (TID) and displacement damage effects. TID produces threshold voltage shifts on the CCD gates and displacement damage reduces the CTE, increases the dark current, produces dark current nonuniformities and creates random telegraph noise in individual pixels. In addition to these long term effects, cosmic rays, trapped protons and secondaries produce transients also interfere with device operation on orbit.

There are many techniques used to measure the CTE of a CCD, each with their own advantages and applicability to a particular situation. One popular method due to it's inherent reproducibility is the x-ray technique. X-rays are employed to produce well-defined and well separated charge packets which are read out and their intensity and

location plotted. This technique is capable of discerning very small changes in CTE, but is not appropriate to use in cases of severe CTE degradation. Signal charge packets may also be introduced electrically in some CCD designs [Mohs74]. Optical CTE measurement techniques include the use of bar patterns, the extended edge pixel response (EPER), the first pixel response (FPR) and various other techniques involving spot illumination of a CCD. The EPER method employs a flat field illumination and overclocks the array to measure the deferred charge. In contrast, FPR measures the charge missing from the leading edge of a flat field image. A detailed comparison of the X-ray, EPER and FPR CTE measurement techniques can be found in [Wacz01].

It is important to note that the CTE is extremely application dependent. It is nontrivial to predict on-orbit CCD instrument performance based on a particular CTE measurement made on the ground. For example, scenes with a diffuse background charge provide some degree of "fat zero" that help to keep the radiation induced traps filled so that they do not remove charge from a signal packet. In contrast, astronomy missions may stare using long integration times to integrate sparse low level signals. In such a case, the radiation induced traps remove charge from the signal packets resulting in a reduction in CTE and the associated image smearing.   The CTE is also dependent on measurement conditions such as temperature, readout rate, clock overlap, signal level and CCD architecture.

Another important CCD parameter to characterize is the dark current nonuniformity which always exists as a result of the statistics associated with the collision kinematics as the incoming proton interacts with the Si lattice. The dark current nonuniformity can characterized by analysis of full frame data acquired using correlated double sampling. A pixel by pixel subtraction of the dark frames before and after irradiation is used to generate dark current histograms which can then be analyzed further. The nonuniformity can be significantly increased in devices with high electric field regions which can produce very high dark current pixels through electric field enhanced emission.

Finally, the transient response of a CCD can also be of interest. Heavy ion and proton transient effects such as charge spreading may be assessed by acquiring sparse hit frames at a proton accelerator. The incoming particle flux is reduced so that there are many fewer than one strike per pixel during the integration and readout times of a particular device so that individual transients can be studied. A series of dark frames are acquired prior to exposure to the beam to provide a baseline to subtract out all effects save the transients themselves.

In order to design an appropriate proton ground test, it is essential to request the expected proton energy spectrum associated with the mission lifetime. Once one or more proton test energies have been chosen for a particular space mission, the relevant MeV-equivalent fluences for a particular mission can be calculated using the calculated NIEL and the differential proton fluence spectrum, for the time period of interest. Monoenergetic proton energies between 40-63 MeV are typically used to assess

displacement damage in CCDs. The large majority of proton test plans call for passive exposures with the detailed characterization occurring back at the laboratory. Often test plans are driven by the available number of devices and time constraints. The same device may be utilized to obtain data at multiple fluence levels if one has the time for multiple trips to the proton cyclotron. Otherwise one uses several devices and samples a few key fluences such as one half, one and two times the mission equivalent fluence at the chosen test energy. In addition, transient testing and other specialized live tests may be performed for some programs. It is important to acquire key results using a flight lot CCD.

The primary 'lesson learned' for CCD ground testing is to test your flight lot CCD using techniques and measurement conditions that best represent the application at hand.

VII. Appendix A

Non-Ionizing Energy Loss Rate (NIEL) Concept

It has been shown that the radiation response of many devices can be predicted reasonably well based on calculations of the amount of displacement damage energy imparted to the primary knock-on atoms.[7] The non-ionizing energy loss rate (NIEL) can be calculated analytically from first principles based on differential cross sections and interaction kinematics. NIEL is that part of the energy introduced via both Coulomb (elastic), nuclear elastic, and nuclear inelastic interactions, which produces the initial vacancy-interstitial pairs and phonons (e.g., vibrational energy). NIEL can be calculated using the following analytic expression that sums the elastic and inelastic contributions as:

$$\text{NIEL} = (N/A) \, [\sigma_e T_e + \sigma_i T_i]. \qquad (1)$$

The σ's are total cross sections, the T's are effective average recoil energies corrected for ionization loss using the Lindhard theory [Lind63], N is Avogadro's number, and A is the gram atomic weight of the target material. In the case of compounds, the total NIEL is derived as a superposition (weighted by mole fraction) of the contributions for each atomic component [Zeig84]. Notice that the units of NIEL, (keVcm^2/g), are the same as those for stopping power (or LET) describing energy transfer by ionization and excitation per unit length. Burke has calculated NIEL in silicon for protons and other ions over a broad energy range [Burk86]. More recent calculations by Burke have incorporated improvements in the treatment of the nuclear elastic and inelastic reactions, and the Lindhard correction has been applied to the differential recoil spectrum instead of to the average recoil energy of the target atoms. The more accurate calculation is given by

$$NIEL = N/A \int L[T(\Theta)] T(\Theta) [d\boldsymbol{s}/d\Omega] d\Omega \qquad (2)$$

where $d\sigma/d\Omega$ is the differential cross section for a recoil in direction Θ, $T(\Theta)$ is the recoil energy, and $L[T(\Theta)]$ is the fraction of the recoil energy that goes into displacements [Lind63]. In the case of Si, the maximum amount of displacement damage energy is about 300 keV, regardless of the energy of the recoiling atom. Figure 1 shows both the LET and NIEL for Si as a function of incident proton energy. The most recent published NIEL calculations for Si can be found in the December IEEE Transactions of Nuclear Science [Dale94].

---

[7] See [Mars99] and references therein for a detailed discussion of the experimental basis for the NIEL correlation as well as its limitations. This work provides examples of the NIEL correlation for the specific case of Si sensor arrays.
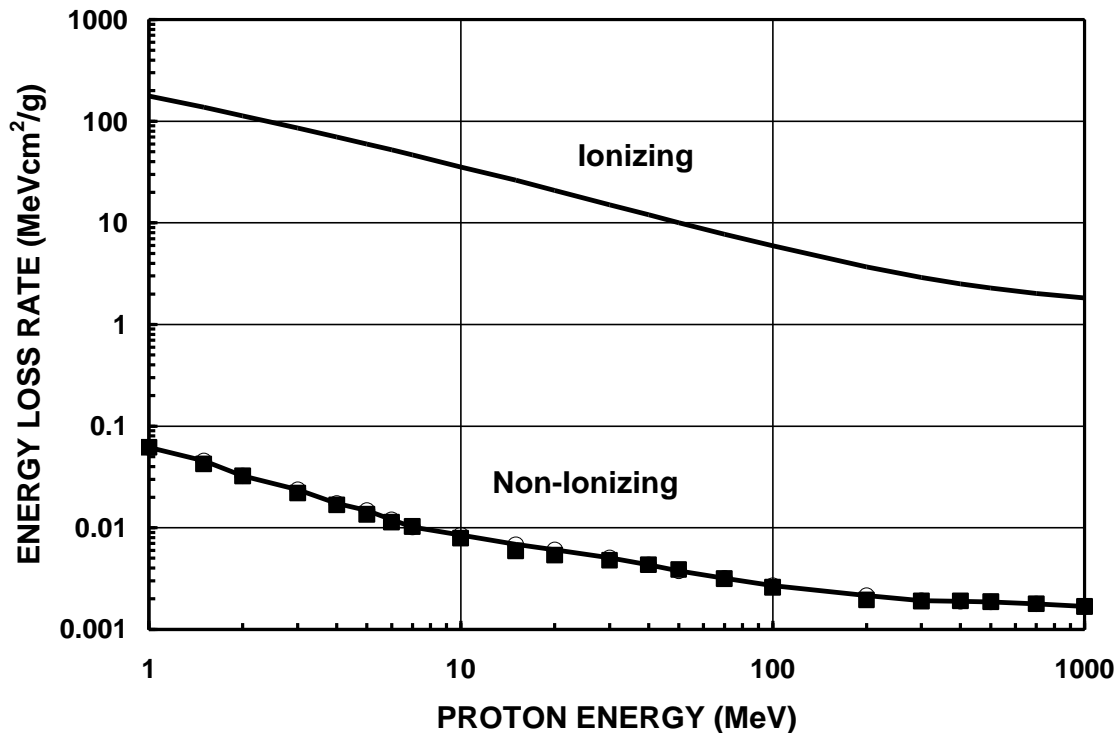
Figure 1   Comparison of the energy loss rate through ionization and excitation of the Si lattice (LET), and through atomic displacements (NIEL) over a wide range of proton energies. The LET was calculated as in [Zeig84], and NIEL as in [Dale94].

The nature of displacement damage as a function of proton energy is governed by the interaction cross sections, and the non-ionizing energy of the PKAs as governed by the Lindhard function. For proton energies below about 10 MeV, Coulomb elastic scattering is by far dominant in Si, and produces atomic recoils with non-ionizing energies in the hundreds of eV. At higher energies, the bend in the curve occurs because nuclear elastic scattering becomes more important resulting in recoils with non-ionizing energies in the tenths of MeV range. As the incident proton energy increases the elastic cross section decreases although it is still larger than the inelastic cross section. By about 100 MeV half of the non-ionizing energy imparted to the Si lattice is from nuclear inelastic reactions with a mean PKA non-ionizing energy that is still about 0.1 MeV (due to the Lindhard partition).

NIEL has also been calculated by other means including Monte Carlo programs such as HETC [Alur91], TRIM [Zeig84] and MCNPX [Jun03]. A comparison between the most recent Burke and CUPID calculations of Si NIEL is discussed in [Dale94]. Although HETC, CUPID and Burke's calculations of the recoil distributions as a function of incident proton energy show similar trends, they differ in details [Dale94]. The TRIM program only includes the Coulombic interactions, so it is not appropriate to use it directly for damage calculations for proton energies above about 8 MeV or so, depending on the target material.

Note that all of the above calculations include a "fudge factor" that accounts for the fact the most of the initially produced vacancy-interstitial pairs recombine and therefore do not produce electrically active defects. For example TRIM is often executed assuming a displacement energy threshold of 25 eV, which is considerably higher than the actual value. This practice helps to account for the efficiency of the initial recombination of the vacancy-interstitial pairs. In other Monte Carlo codes such as MARLOWE, one also has the option to define a radius around each collision point for which all the vacancy-interstitial pairs recombine. In essence, all current NIEL calculations must be scaled to fit the experimental damage factors, unless damage factor ratios are compared. As we shall see, it is the calculation of the energy dependence that is relevant, not the absolute values of NIEL.

VIII. References

[Alur91]   M. Alurralde, M. Victoria, A. Caro, and D. Gavillet, "Nuclear and Damage Effects in Si Produced by Irradiations with Medium Energy Protons," IEEE Trans. Nucl. Sci., Vol. 38, No. 6, pp. 1210-1215, 1991.

[Bang91]   E.K. Banghart, J.P. Lavine, E.A. Trabka, E.T. Nelson, and B.C. Burkey, "A Model for Charge Transfer in Buried-Channel Charge-Coupled Devices at Low Temperature," IEEE Trans. El. Dev., Vol. 38, No. 5, pp. 1162-1173, May 1991.

[Bebe02]   C.J. Bebek, D.E. Groom, S.E. Holland, A. Karcher, W.F. Kolbe, J. Lee, M.E. Levi, N.P. Palaio, B.T. Turko, M.C. Uslenghi, M.T. Wagner, and G. Wang, "Proton radiation damage in high-resistivity n-type silicon CCDs," Proceeding of SPIE, Vol. 4669, pp. 161-171, 2002.

[Burk86]   E.A. Burke, "Energy Dependence of Proton-Induced Displacement Damage in Silicon," IEEE Trans. Nucl. Sci., Vol. 33, No. 6, pp. 1276-1281, 1986.

[Blad00]   "Ultraviolet and Visible Detectors for Future Space Astrophysics Missions: A Report from the Ad-hoc, UV-Visible Detectors Working Group of NASA's Office of Space Science," edited by J. Chris Blades, 2000.

[Burk91]   B. Burke and S. A. Gajar, "Dynamic suppression of interface-state dark current in buried channel CCDs", IEEE Trans. on Electron Devices, vol. 38 no.2, pp. 285-290, 1991.

[Clam02]   M. Clampin, G. Hartig, H.C. Ford, M. Sirianni, G. Meurer, A. Martel, J.P. Blakeslee, G.D. Illingworth, J. Krist, R. Gilliland, and R. Bohlin, "Status for the Advanced Camera for Surveys," 2002 HST Calibration Workshop, Space Telescope Science Institute, October 2002.

[Dale89]   C.J. Dale, P.W. Marshall, E.A. Burke, G.P. Summers, and G.E. Bender, "The Generation Lifetime Damage Constant and its Variance," IEEE Trans. Nucl. Sci., Vol. 36, No. 6, pp. 1872-1881, 1989.

[Dale91]   C.J. Dale and P.W. Marshall, "Displacement Damage in Silicon Imagers for Space Applications," Proc. SPIE, Vol. 1447, pp. 70-86, 1991.

[Dale93]   C. Dale, P. Marshall, B. Cummings, L. Shamey and A. Holland, "Displacement damage effects in mixed particle environments for shielded spacecraft CCDs", IEEE Trans. on Nucl. Sci., vol. 40, no. 6, pp. 1628-1637, Dec. 1993.

[Dale94]   C.J. Dale, L. Chen, P.J. McNulty, P.W. Marshall, and E.A Burke, "A Comparison of Monte Carlo and Analytic Treatments of Displacement Damage in Microvolumes," IEEE Trans. Nucl. Sci., Vol. 41, No. 6, pp. 1974-1983, 1994.

[Gall98]   D.Gallagher, R. Demara, G. Emerson, W. Frame and A. Delamere, "Monte Carlo model for describing charge transfer in irradiated CCDs", Proc SPIE, vol. 3301, pp. 80-88, 1998.

[Goli00]   Private communication with David Golomowski, Johns Hopkins University, 2000.

[Greg93]   J.A. Gregory, B.E. Burke and M.J. Cooper, Solid State Research, Quarterly Technical Report (ESC-TR-92-149), Lincoln Laboratory, MIT, 31 Jan 1993, pp. 48-50.

[Hard98]   T. Hardy, R. Murowinski, and M.J. Deen, "Charge Transfer Efficiency in Proton Damaged CCD's," IEEE Trans. Nucl. Sci., vol. 45, no. 2, pp. 154-163, 1998.

[Holl91]   A.D. Holland, "Annealing of proton-induced displacement damage in CCDs for space use," Inst. Phys. Conf. Ser. 121, pp. 33-40, 1991.

[Holm96]   A.Holmes-Seidle, A. Holland and S. Watts, "The impact of space protons in x-ray sensing with charge coupled devices (CCDs)", IEEE Trans. on Nucl. Sci., vol. 43, no. 6, pp. 2998-3003, Dec. 1996.

[Holt95]   J. Holtzmam et al., "The performance and calibration of WFPC2 on the Hubble Space Telescope", Publ. Astron. Soc. Pac., vol. 107, pp.156-178, 1995.

[Hopk91]   G.R. Hopkinson, "Co60 Radiation Testing of THX31160 and TH7863 CCDs for the Silex Porgramme," Final Report, ESA Contract No. 7787/88/NL/DG, March 1991.

[Hopk92]   G.R. Hopkinson, "Cobalt-60 and Proton Radiation Effects on Large Format, 2-D, CCD Arrays for an Earth Imaging Application," IEEE Trans. Nucl. Sci., Vol. 39, No. 6, pp. 2018-2025, 1992.

[Hopk93]   I.H. Hopkins and G.R. Hopkinson, "Random Telegraph Signals from Proton-Irradiated CCDs," IEEE Trans. Nucl. Sci., Vol. 40, No. 6, pp. 1567-1574, 1993.

[Hopk94] I.H. Hopkins, G.R. Hopkinson, and B. Johlander, "Proton-Induced Charge Transfer Degradation in CCDs for Near-Room Temperature Applications," IEEE Trans. Nucl. Sci., Vol. 41, No. 6, pp. 1984-1990, 1994.

[Hopk95]   I.H. Hopkins and G.R. Hopkinson, "Further Measurements of Random Telegraph Signals in Proton-Irradiated CCDs," IEEE Trans. Nucl. Sci., Vol. 42, No. 6, pp. 2074-2081, 1995.

[Hopk96]   G. R. Hopkinson, C. J. Dale, and P. W. Marshall, "Proton effects in CCDs", IEEE Trans. on Nucl. Sci., Vol. 43, no. 2, pp. 614-627, Apr. 1996.

[Hopk99]   G. R. Hopkinson, " Proton damage effects on p-channel CCDs", IEEE Trans. on Nucl. Sci., vol. 46, no. 6, pp. 1790 -1796, Dec. 1999.

[Hopk00]   G. R. Hopkinson, "Proton-induced changes in CTE for n-channel CCDs and the effect on star tracker performance", IEEE Trans. on Nucl. Sci., vol. 47, no. 6, pp. 2460-2465, Dec. 2000.

[Hopk01]   G.R. Hopkinson, "Proton-Induced CCD Charge Transfer Degradation at Low-Operating Temperatures," IEEE Trans. Nucl. Sci., Vol. 48, No. 6, pp. 1790-1795, 2001.

[Jane91]   J. Janesick, G. Soli, T. Elliott, and S. Collins, "The Effects of Proton Damage on Charge-Coupled Devices," Proc. SPIE, Vol. 1447, pp. 87-108, 1991.

[Jane95]   J. Janesick, T. Elliott, R. Winzenread, J. Pinter, and R. Dyck, "Sandbox CCD's," Proc. SPIE, vol. 2415, pp. 2-42, 1995.

[Jane01]   J.R. Janesick, "Scientific Charge-Couple Devices," SPIE Press, Bellingham, WA, 2001.

[John00]   S. Johnson, A. Waczynski, E. Polidan, P. Marshall, and R. Reed, "An Analysis of Charge Transfer Efficiency Noise on Proton-Damaged CCDs for the Hubble Space Telescope Wide Field Camera 3," Proc. SPIE, vol. , pp., 2000.

[Jun03]   I. Jun, M.A. Xapsos, S.R. Messenger, E.A. Burke, R.J. Walters, G.P. Summers and T.M. Jordan, "Proton NonIonizing Energy Loss (NIEL) for Device Applications," presented at NSREC 2003.

[Kimb00]   R. A. Kimble, P. Goudfrooij and R. L. Gilliland, "Radiation damage effects on the CCD detector of the space telescope Imaging spectrograph", Proc. SPIE, vol. 4013, pp. 532-545, July 2000.

[Lieb01]   C.C. Liebe," Charged particle-induced noise in camera systems", IEEE Trans. on Nucl. Sci., vol. 48, no. 4, pp. 1541 -1549, Aug. 2001.

[Lind63]   J. Lindhard, V. Nielsen, M. Scharff, and P. Thomsen, "Integral Equations Governing Radiation Effects (Notes on Atomic Collisions, III)," Mat. Fys. Medd. Dan. Vid. Selsk., Vol. 33, No. 10, p.1, 1963.

[Lomh90]   T.S. Lomheim, R.M. Shima, J.R. Angione, W.F. Woodward, D.J. Asman, R.A. Keller, and L.W. Schumann, "Imaging Charged-Coupled Device (CCD) Transient Response to 17 and 50 MeV Proton and Heavy Ion Irradiation," IEEE Trans. Nucl. Sci., Vol. 37, No. 6, pp. 1876-1885, 1990.

[Mars80]   P. W. Marshall, C. J. Dale, E. A. Burke, G. P. Summers, and G.E. Bender, "Displacement Damage Extremes in Silicon Depletion Regions," IEEE Trans. Nucl. Sci., Vol. 36, No. 6, pp. 1831-1839, 1989.

[Mars90]   P.W. Marshall, C.J. Dale, E.A. Burke, "Proton-Induced Displacement Damage Distributions and Extremes in Silicon Microvolumes," IEEE Trans. Nucl. Sci., Vol. 37, No. 6, pp. 1776-1783, 1990.

[Mars99]   P.W. Marshall and C.J. Marshall, "Proton Effects and Test Issues for Satellite Designers," IEEE NSREC Short Course, July 1999, and references therein.

[Mohs74]   A.M. Mohsen and M.F. Tompsett, "The Effects of Bulk Traps on the Performance of Bulk Channel Charge-Coupled Devices," IEEE Trans. El. Dev., vol. ED-21, no. 11, pp. 701-712, Nov. 1974.

[Phil02]   R. H. Philbrick, " Modeling the impact of preflushing on CTE in proton irradiated CCD-based detectors", IEEE Trans. on Nucl. Sci., vol. 49, no. 2, pp. 559 -567, April 2002.

[Pick03]   J.C. Pickel, H.A. Kalma, G.R. Hopkinson, and C.J. Marshall, "Radiation Effects on Photonics – A Historical Perspective," to be published in IEEE Trans. Nucl. Sci., 2003.

[Poli03]   Elizabeth J. Polidan, Augustyn Waczynski, Paul W. Marshall, Scott D. Johnson, Cheryl Marshall, Robert A. Reed, Randy A. Kimble, Gregory Delo, David Schlossberg, Anne Marie Russell, Terry Beck, Yiting Wen, John Yagelowich, Robert J. Hill, and Edward J. Wassell, "Hot pixel behavior in WFC3 CCD detectors irradiated under operational conditions," to be published in SPIE Astronomical proceedings [2003].

[Prig00]   G. Prigozhin et al. "Characterization of the radiation damage in the Chandra X-ray CCDs". Proc. SPIE, vol. 4140, pp. 123-134, Aug. 2000.

[Reis02]   A. Reiss, "Growth of Hot Pixels and Degradation of CTE for ACS," 2002 HST Calibration Workshop, Space Telescope Science Institute, October 2002.

[Robb92]   M. Robbins, "Radiation Damage Effects in Charge Coupled Devices," Ph.D. Dissertation, Brunel University, 1992.

[Robb93]   M. S. Robbins, T. Roy, S. J. Hedges, A. Holmes-Siedle, A.K McKemey, and S. J. Watts, "Quality control and monitoring of radiation damage in charge coupled

devices at the Stanford Linear Collider", IEEE Trans. on Nucl. Sci., vol. 40, no. 6, pp. 1561 -1566, Dec. 1993

[Saks80]   N.S. Saks, "A technique for suppressing dark current generated by interface states in buried channel CCD imagers", IEEE Electron device letters, vol. 1, no. 7, July 1980.

[Sprat97] J.P. Spratt, B.C. Passenheim, and R.E. Leadon, "The Effects of Nuclear Radiation on P-Channel CCD Imagers," IEEE Radiation Effects Data Workshop, pp. 116-121. 1997.

[Srou86]   J.R. Srour, R.A. Hartman, and K.S. Kitazaki, "Permanent Damage Produced by Single Proton Interactions in Silicon Devices," IEEE Trans. Nucl. Sci., Vol. 33, No. 6, pp. 1597-1604, 1986.

[Srou89]   J.R. Srour and R.A. Hartman, "Enhanced Displacement Damage Effectiveness in Irradiated Silicon Devices," IEEE Trans. Nucl. Sci., Vol. 36, No. 6, pp. 1825-1830, 1989.

[VanT94]   W. Van Toren and J. Bisschop, "Complete characterization of dark current in frame transfer image sensors," Philips J. Res., vol. 48, pp. 207-231, 1994.

[Yama97]   A. Yamashita, T. Dotani, M. Bautz, G. Crew, H. Ezuka, K. Gendreau, T. Kotani, K. Mitsuda, C. Otani, A. Rasmussen, G. Ricker and H. Tsunemi, "Radiation damage to charge coupled devices in the space environment", IEEE Trans. on Nucl. Sci., vol. 44, no. 3, pp. 847-853, Jun. 1997.

[Wacz01]   Waczynski, E. J. Polidan, P. W. Marshall, R. A. Reed, S. D. Johnson, R. J. Hill, G. S. Delo, E. J. Wassell and E. S. Cheng, "A comparison of charge transfer efficiency measurement techniques on proton damaged CCDs for the Hubble Space Telescope Wide-Field Camera 3", IEEE Trans. on Nucl. Sci., vol. 48, no. 6, pp 1807-1814, Dec. 2001.

[Whit02]   B. Whitmore and I. Heyer, "Charge Transfer Efficiency for Very Faint Objects and a Reexamination of the Long-vs.-Short Problem for the WFPC2," 2002 HST Calibration Workshop, Space Telescope Science Institute, October 2002.

[Zeig84]   J.F. Zeigler, J.P. Biersack, and U. Littmark, The Stopping and Range of Ions in Solids, Pergamon Press, New York, 1984.